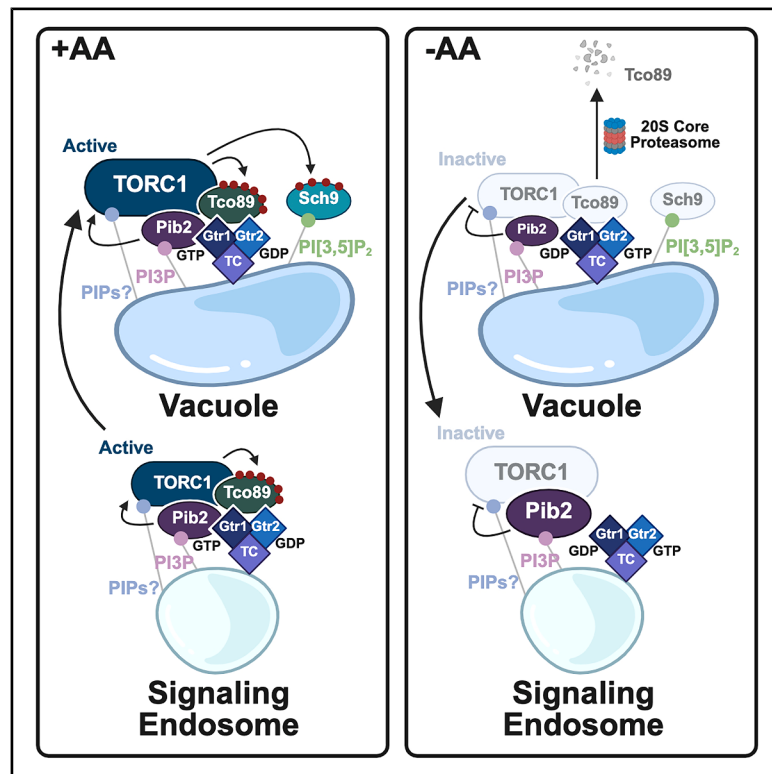


TORC1 autonomously controls its spatial partitioning via the Rag GTPase tether Tco89

Graphical abstract



Authors

Raffaele Nicastro, Marie-Pierre Pélis-Gulli, Marco Caligaris, ..., Riko Hatakeyama, Jörn Dengjel, Claudio De Virgilio

Correspondence

claudio.devirgilio@unifr.ch

In brief

Rag GTPases mediate amino acid signals to control TORC1. Nicastro et al. show that yeast Tco89 tethers TORC1 to Rag GTPases to enable it to control vacuolar effectors. TORC1 phosphorylates and stabilizes Tco89, reinforcing this interaction and preventing TORC1 from relocating to endosomes and being separated from these effectors.

Highlights

- Amino acids activate TORC1 through the Rag GTPases at endolysosomal membranes
- Tco89 structurally tethers TORC1 to Rag GTPases, thus enabling control of vacuolar effectors
- TORC1 reinforces this interaction by directly phosphorylating and stabilizing Tco89
- TORC1 inactivation and Tco89 decay shift TORC1 to endosomes, away from vacuolar effectors



Article

TORC1 autonomously controls its spatial partitioning via the Rag GTPase tether Tco89

Raffaele Nicastro,^{1,4} Marie-Pierre Pélis-Gulli,¹ Marco Caligaris,¹ Malika Jaquenoud,¹ Ladislav Dokládal,¹ Josephine Alba,¹ Farida Tripodi,² Benjamin Pillat,¹ Melanie Brunner,¹ Michael Stumpe,¹ Kenji Muneshige,³ Riko Hatakeyama,³ Jörn Dengjel,¹ and Claudio De Virgilio^{1,5,*}

¹Department of Biology, University of Fribourg, Fribourg, Switzerland

²Department of Biotechnology and Biosciences, University of Milano-Bicocca, Milano, Italy

³Institute of Medical Sciences, School of Medicine, Medical Sciences & Nutrition, University of Aberdeen, Aberdeen, UK

⁴Present address: Department of Biological Sciences, University of Limerick, Limerick, Ireland

⁵Lead contact

*Correspondence: claudio.devirgilio@unifr.ch

<https://doi.org/10.1016/j.celrep.2025.115683>

SUMMARY

The eukaryotic target of rapamycin complex 1 (TORC1) kinase is a homeostatic regulator of growth, integrating nutritional cues at the endolysosomal compartment. Amino acids activate mammalian TORC1 (mTORC1) through the Rag GTPases that recruit it to lysosomes via a short domain within the mTORC1 sub-unit Raptor. Intriguingly, this “Raptor claw” domain is absent in Kog1, the Raptor ortholog in yeast. Instead, as we show here, yeast utilizes the fungal-specific Tco89 to tether TORC1 to active Rag GTPases. This interaction enables TORC1 to precisely calibrate the activity of the S6K1-related effector kinase Sch9 in response to amino acid availability. TORC1 stabilizes Tco89 by phosphorylation, and its inactivation causes swift Tco89 proteolysis, provoking a redistribution of TORC1 from the vacuole to signaling endosomes and its spatial separation from Sch9. Thus, TORC1 not only operates in spatially distinct subcellular pools but also controls its own quantitative distribution between these pools to economize energy resources under fluctuating nutrient conditions.

INTRODUCTION

Eukaryotic cells have evolved intricate signaling pathways to sense and respond to fluctuating environmental conditions, enabling precise control of metabolism, growth, proliferation, and survival. A central node in this network is the highly conserved target of rapamycin complex 1 (mTORC1 in mammals and TORC1 in yeast), a master regulator of cell growth and metabolism. TORC1 integrates hormonal, growth factor, energy, and nutritional cues, particularly amino acids, to coordinate anabolic processes such as protein translation and inhibit catabolic processes like macroautophagy.¹ Dysregulation of mTORC1 in humans is implicated in a range of diseases, including cancer, obesity, type 2 diabetes, and neurodegeneration,^{2,3} highlighting its profound impact on human health. mTORC1 comprises a dimer of the protein kinase mTOR, Raptor (regulatory-associated protein of mTOR), mLst8 (mammalian lethal with Sec thirteen 8), and two additional subunits, PRAS40 (proline-rich Akt substrate of 40 kDa) and DEPTOR (DEP domain-containing mTOR-interacting protein).^{4–6} In *Saccharomyces cerevisiae*, the TORC1 dimer is composed of Tor1 (or Tor2), Kog1 (Raptor ortholog), Lst8, and the yeast-specific 89-kDa subunit Tco89.⁴ Tco89, a non-essential protein initially identified in a screen for osmotic-stress-related glycerol uptake defects,⁷ is important for maintaining cell integrity.⁸ Loss of Tco89 also results in hypersensitivity to rapamycin

and caffeine, and *tco89Δ* cells phenocopy *Tor1*-deficient cells, indicating a positive role for Tco89 in TORC1 signaling.⁸ This is further supported by the requirement of Tco89 for the selective vacuolar import and degradation of fructose-1,6-bisphosphatase (FBPase), a known TORC1-dependent process.^{9,10} Despite the widespread conservation of Tco89 orthologs in fungi, its precise role within TORC1 has remained enigmatic.

TORC1 functions at lysosomal/vacuolar and endosomal surfaces in eukaryotes, interacting with conserved heterodimeric Rag GTPases (RagA/B bound to RagC/D in mammals and Gtr1 bound to Gtr2 in yeast).^{11,12} These heterodimers associate with the pentameric Ragulator complex in mammals or the EGO (exit from rapamycin-induced growth arrest) ternary complex (EGO-TC) in yeast,^{13–15} which are anchored to lysosomal/vacuolar and endosomal membranes via an N-terminally lipidated subunit.^{15–17} The Rag GTPases cycle between an active state (RagA/B/Gtr1 GTP-bound and RagC/D/Gtr2 GDP-bound) and an inactive state (with the opposite nucleotide loading). These nucleotide states are regulated by conserved GTPase-activating protein (GAP) complexes, such as mammalian GATOR1/yeast SEACIT and mammalian FNIP-FLCN/yeast Lst4-Lst7, acting on RagA/B/Gtr1 and RagC/D/Gtr2, respectively.^{18–25} These complexes integrate signals from distinct cytosolic and lysosomal/vacuolar amino acid pools through different mechanisms.^{1,3,11}



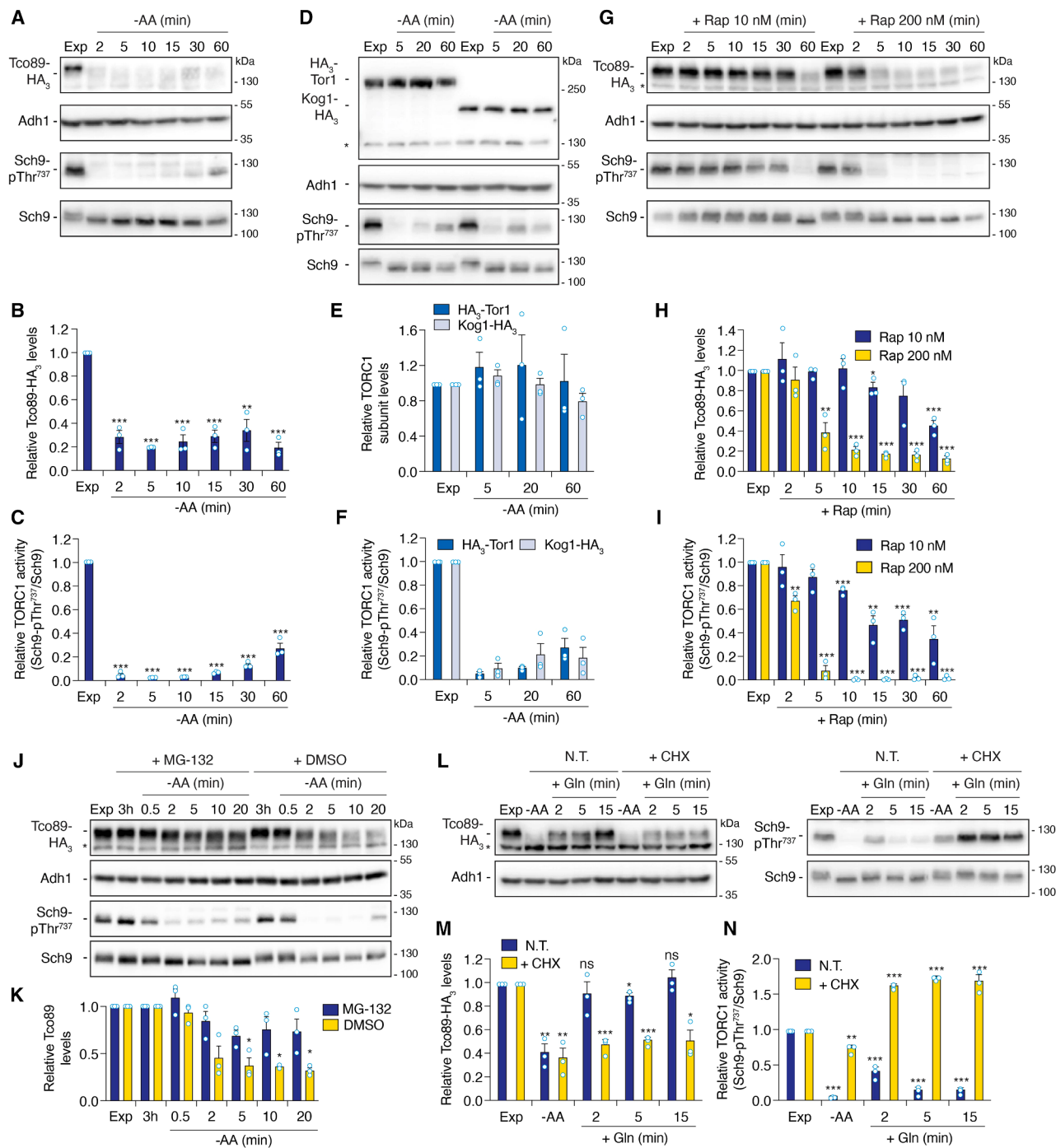


Figure 1. TORC1 inhibits proteolysis of Tco89

(A) Tco89 levels rapidly decrease upon amino acid starvation. Cells expressing Tco89-HA₃ were grown exponentially in synthetic complete medium (SC) (Exp), starved for amino acids (-AA), and collected at indicated time points. Lysates were analyzed by immunoblotting with anti-hemagglutinin (HA), anti-Adh1, anti-Sch9-pThr⁷³⁷, and anti-Sch9 antibodies. See also Figure S1.

(B) and (C) Relative Tco89-HA₃ levels (B) and TORC1 activities (C) quantified from (A) (HA/Adh1 and Sch9-pThr⁷³⁷/Sch9 ratios, respectively, normalized to Exp; means ± SEM, $n = 3$).

(D) Tor1 and Kog1 levels are unaffected by amino acid starvation. Cells expressing HA₃-Tor1 or Kog1-HA₃ were grown (Exp), starved for amino acids (-AA), and analyzed as in (A).

(E) and (F) Relative HA₃-tagged TORC1 subunit levels (E) and TORC1 activities (F) quantified from (D) as in (B) and (C).

(legend continued on next page)

In the presence of amino acids, active Rag GTPases recruit mTORC1 to lysosomes, where it is allosterically activated by the small GTPase Rheb (Ras homolog enriched in brain),^{26–29} leading to the phosphorylation of effectors such as S6K1 (S6 kinase 1) and 4E-BP1 (eukaryotic initiation factor 4E-binding protein 1), which bind mTORC1 through their TOS (TOR signaling) motif.^{30–32} Rheb activity is responsive to growth factors and energy levels, integrated by the Rheb GAP complex Rhebulator.^{6,29,30,33–36} In addition to this canonical mechanism, Rag GTPases also recruit specific substrates, such as the transcription factors TFEB and MiT-TFE (key regulators of lysosome biogenesis and autophagy),^{37–41} for mTORC1-mediated phosphorylation. In budding yeast, Rag GTPases are not strictly required for TORC1 localization to endolysosomal membranes, and the Rheb ortholog Rhb1 is dispensable for normal TORC1 regulation of its vacuolar membrane-associated effector Sch9 (a protein kinase related to mammalian S6K1 and central to calibrating metabolic and stress responses).^{42,43} Therefore, the mechanistic details of Rag GTPase-mediated TORC1 regulation in budding yeast have remained largely undefined.

Here, we demonstrate that Tco89 functions as a structural tether, assembling TORC1 with active Rag GTPases to enable TORC1-mediated phosphorylation and activation of vacuolar membrane-localized Sch9. Mechanistically, TORC1 reinforces this interaction through a feedforward loop by directly phosphorylating and stabilizing Tco89. Critically, upon amino acid starvation, TORC1 inactivation triggers rapid Tco89 degradation, which, similar to Tco89 deletion, leads to TORC1 redistribution from the vacuolar surface to signaling endosomes, effectively separating TORC1 from its target Sch9. These findings illuminate the previously enigmatic role of Tco89 and define a mechanism for Rag GTPase-mediated TORC1 regulation in yeast, highlighting the remarkable capacity of TORC1 to autonomously modulate its spatial proximity to its effectors.

RESULTS

TORC1 inhibits proteolysis of Tco89

Prior work identified 23 rapamycin-sensitive phosphoresidues within Tco89 *in vivo*,^{44,45} of which we confirmed that 20 are also phosphorylated by TORC1 using *in vitro* kinase assays (Table S1 and Hu et al.⁴⁴). Consistent with this direct phosphorylation, λ phosphatase treatment of immunopurified Tco89-HA₃ from exponentially growing cells resulted in a discernible increase in SDS-PAGE mobility. Importantly, this mobility shift was prevented by prior λ phosphatase inactivation (via heat or

chemical inhibition; Figure S1A). *In vivo*, Tco89-HA₃ migrated as a single band in exponentially growing cells, and its expression, unlike *TCO89* deletion, did not perturb TORC1-mediated phosphorylation of the established TORC1 substrate Sch9-Thr⁷³⁷ (Figures S1B and S1C).^{46,47} Strikingly, amino acid starvation, which rapidly abrogated TORC1 activity (i.e., relative Sch9-pThr⁷³⁷/Sch9 levels), induced a rapid increase in Tco89-HA₃ SDS-PAGE mobility (likely reflecting dephosphorylation) coupled with a concomitant decrease in Tco89-HA₃ abundance (Figures 1A–1C). These observations were consistent across GFP- and myc₁₃-tagged Tco89 variants (Figures S1D–S1I). Control experiments established that only Tco89-HA₃ levels, and not HA₃-tagged Tor1 or Kog1 levels, were sensitive to amino acid starvation (Figures 1D–1F). This finding aligns with proteomic analyses demonstrating a specific decrease in Tco89, but not other core TORC1 subunits, following prolonged amino acid starvation (6 h).⁴⁸ Furthermore, treatment of exponentially growing cells with increasing rapamycin concentrations (10 and 200 nM) resulted in TORC1 inactivation and a corresponding decrease in Tco89-HA₃ abundance, mirroring the established rapamycin dose- and time-dependent inhibition of TORC1 (Figures 1G–1I). Therefore, the observed decrease in Tco89-HA₃ protein levels is a direct consequence of TORC1 inhibition.

The rapid loss of Tco89-HA₃ upon amino acid starvation was not attributable to transcriptional regulation, as *TCO89* (and *KOG1*) transcript levels remained unchanged, while *TOR1* transcripts exhibited a modest increase and ribosomal protein gene transcripts (e.g., *RPL6B*, *RPL9A*, and *RPP0*) robustly decreased, as expected (Figure S1J).⁴⁹ Coupled with our observation that dephosphorylated Tco89 was not intrinsically unstable *in vitro* (Figure S1A), these data suggested that Tco89 undergoes rapid proteolysis in amino-acid-starved cells. Known proteolytic processes such as non-selective bulk macroautophagy,⁵⁰ selective cytoplasm-to-vacuole (Cvt) autophagy,⁵¹ or the vacuolar membrane protein recycling and degradation (vReD) pathway⁵² were not involved in Tco89 degradation, as loss of essential regulators or drivers of these processes (i.e., the Atg1 kinase, the receptor protein Atg19, or the specificity factor Ssh4, respectively) did not significantly affect amino-acid-starvation-induced Tco89 degradation (Figures S1K and S1L). We therefore hypothesized that Tco89 degradation is proteasome mediated, primarily in its dephosphorylated state. Consistent with this, both proteasome inhibition by MG-132 in *erg6Δ pdr5Δ* cells (exhibiting increased drug permeability and reduced efflux)^{53,54} strongly (Figures 1J and 1K) and heat inactivation of the temperature-sensitive 20S core proteasome (CP) subunit Pup1^{ts} partially (Figure S1M)

(G) Tco89 levels decrease upon rapamycin treatment. Cells expressing Tco89-HA₃ were grown exponentially (Exp), treated with 10 or 200 nM rapamycin (Rap), collected at indicated times, and analyzed as in (A).

(H and I) Relative Tco89-HA₃ levels (H) and TORC1 activities (I) quantified from (G) as in (B) and (C).

(J) Proteasome inhibition protects Tco89 from degradation. Cells (*erg6Δ pdr5Δ*) expressing Tco89-HA₃ were grown exponentially in SC (Exp), pre-treated with DMSO (vehicle, +DMSO) or 50 μM MG-132 (+MG-132) for 3 h, and then starved for amino acids (−AA) in the presence of DMSO or MG-132 and collected at indicated time points. Analysis as in (A).

(K) Relative Tco89-HA₃ levels quantified from (J) as in (B).

(L) Reestablishment of Tco89 levels following amino acid stimulation of starved cells requires *de novo* protein synthesis. Cells expressing Tco89-HA₃ were grown exponentially in SC (Exp) and then starved for amino acids (−AA; 20 min) without (N.T.; not treated) or with 25 μg/mL cycloheximide (+CHX). Glutamine (3.3 mM; +Gln) was resupplemented for the indicated times. Analysis as in (A).

(M and N) Relative Tco89-HA₃ levels (M) and TORC1 activities (N) quantified from (L) as in (B) and (C). ns, not significant.

Asterisks in (D), (G), (J), and (L): cross-reacting band. *p < 0.05, **p < 0.005, and ***p < 0.0005 (paired Student's t test, relative to control).

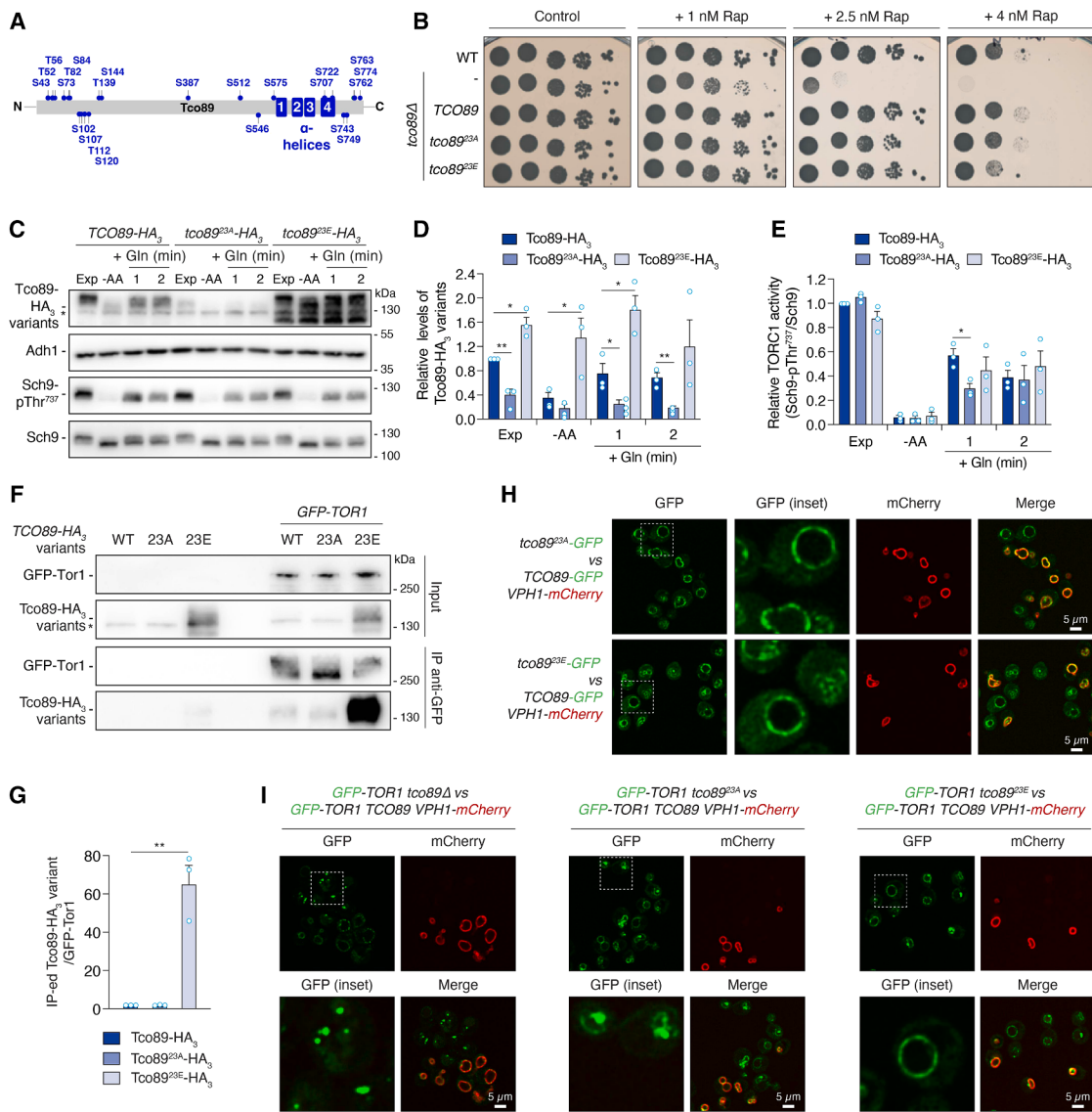


Figure 2. TORC1-target residues balance Tco89 stability

(A) Schematic presentation of Tco89 with C-terminal α helices (1–4) and 23 *in vivo* TORC1-sensitive phosphoresidues, all of which, except Ser¹⁰², Ser¹¹², and Ser¹³⁹, were found to be also targeted by TORC1 *in vitro*.

(B) Phosphomimetic (glutamate; E) but not serine- or threonine-to-alanine (A) mutations of the 23 TORC1 sites in Tco89 cause mild rapamycin sensitivity. Wild-type (WT), *tco89*^Δ, *tco89*^{23A}, and *tco89*^{23E} cells were grown exponentially, spotted (10-fold serial dilutions) on SD-LHUAW plates without (control) or with rapamycin (+Rap; concentrations indicated), and grown for 3 days at 30°C. See also Figure S2.

(C) TORC1-target residues in Tco89 control its abundance. WT, *tco89*^{23A}, and *tco89*^{23E} cells expressing HA₃-tagged Tco89 variants were grown exponentially in SC (Exp), starved for amino acids (-AA; 20 min), and refed with glutamine (3.3 mM; +Gln). Lysates were analyzed as in Figure 1A. Asterisk: cross-reacting band.

(D and E) Relative Tco89-HA₃ variant levels (D) and TORC1 activities (E) quantified from (C) (as in Figures 1B and 1C, respectively). In (D), all *Tco89*^{23E}-HA₃ isoforms (excluding the cross-reacting band marked with an asterisk that is present in untagged strains; Figure S1B) were quantified.

(F) *Tco89*^{23E} exhibits excessive affinity for Tor1. WT and GFP-Tor1 cells expressing Tco89-HA₃ variants were grown exponentially in SC. Lysates were equilibrated for protein concentration (input) and subjected to immunoprecipitation with anti-GFP magnetic beads (IP anti-GFP). Immunoblotting was performed with anti-HA and anti-GFP antibodies.

(G) Relative Tco89-HA₃ variant/GFP-Tor1 levels from (F), normalized to Tco89-HA₃/GFP-Tor1 (means \pm SEM, $n = 3$).

(H) Subcellular localization of GFP-tagged Tco89^{23A/23E} variants. Exponentially growing (on SC) cells expressing Tco89^{23A}-GFP or Tco89^{23E}-GFP were mixed with cells co-expressing Tco89-GFP and Vph1-mCherry and visualized by confocal fluorescence microscopy. Scale bars: 5 μ m.

(I) GFP-Tor1 localization in cells expressing no Tco89, *Tco89*^{23A}, or *Tco89*^{23E}. Cells co-expressing GFP-Tor1 and the indicated Tco89 variants were mixed with cells co-expressing GFP-Tor1, Tco89, and Vph1-mCherry and visualized as in (H). GFP-Tor1 foci were observed in 28% \pm 8% of WT ($n = 377$), 100% of *tco89*^Δ ($n = 320$), 94% \pm 4% of *tco89*^{23A} ($n = 253$), and 75% \pm 9% of *tco89*^{23E} cells ($n = 364$). Scale bars: 5 μ m.

* $p < 0.05$, ** $p < 0.005$, and *** $p < 0.0005$ (paired Student's *t* test relative to control).

prevented Tco89-HA₃ degradation during amino acid starvation. To assess the role of ubiquitination, we generated a Tco89^{K58R}-HA₃ allele, replacing all 58 lysines with arginines. This variant was still rapidly degraded upon amino acid starvation (Figure S1N). Therefore, Tco89 is degraded by the 20S CP, but in a lysine-ubiquitination-independent manner. This aligns with existing literature suggesting that intrinsically disordered region (IDR)-containing proteins, among which are many key signaling proteins with essential roles in cell-cycle progression and growth control, are susceptible to ubiquitin-independent 20S CP degradation.^{55,56} Tco89, possessing a large IDR (spanning 87.5% of the protein according to AlphaFold), may undergo such degradation, potentially induced by its dephosphorylation (see below). Further supporting this, heat inactivation of the temperature-sensitive 19S proteasome regulatory particle (RP) subunit Rpn5^{ts}, which compromises binding and delivery of ubiquitinated proteins to the 20S CP, caused accumulation of ubiquitinated proteins, as expected, but did not affect Tco89-HA₃ degradation during amino acid starvation (Figure S1O).

Finally, glutamine-driven, transient TORC1 reactivation in amino-acid-starved cells²³ restored the slowly migrating Tco89-HA₃ isoform to levels comparable to those observed in exponentially growing cells (Figures 1L–1N). Critically, this effect was blunted by pre-treatment with the translation elongation inhibitor cycloheximide, which, as previously reported, hyperactivated TORC1.^{16,46} Thus, the disappearance of Tco89-HA₃ in amino-acid-starved cells is a consequence of protein degradation, and its reappearance upon glutamine stimulation requires *de novo* protein synthesis. Taken together, these results demonstrate that Tco89 is subject to post-translational phosphorylation, presumably by TORC1 itself, which protects it from proteasome-dependent degradation.

TORC1 promotes its own function through Tco89 phosphorylation

To test whether TORC1-mediated Tco89 phosphorylation protects it from degradation, we generated *tco89Δ* strains expressing either genetically integrated wild-type (WT) Tco89 or alleles in which the 23 previously identified rapamycin-sensitive phosphothreonines (pThr) and phosphoserines (pSer) were replaced with alanines (23A) or phosphomimetic glutamates (23E) (Figure 2A). Both alleles, *tco89^{23A}* and *tco89^{23E}*, complemented the rapamycin hypersensitivity of *tco89Δ* cells, although *tco89^{23E}* cells exhibited slightly greater rapamycin sensitivity than WT and *tco89^{23A}* cells (Figure 2B). In line with a role for phosphorylation in regulating Tco89 stability, HA₃-tagged Tco89^{23A} and Tco89^{23E} protein levels, but not mRNA levels (Figure S2A), were significantly decreased and increased, respectively, in exponentially growing cells (Figures 2C and 2D). Critically, amino acid starvation, which leads to TORC1 inactivation, further reduced Tco89^{23A}-HA₃ levels but did not significantly affect Tco89^{23E}-HA₃ levels (Figures 2C–2E). Notably, a fraction of Tco89^{23E}-HA₃ migrated more rapidly in SDS gels, and amino acid starvation accelerated the migration of the slowest migrating Tco89^{23E}-HA₃ pool. This observation suggests the existence of distinct Tco89 proteoforms with amino-acid-sensitive phosphoresidues that were not detected by mass spectrometry. Nevertheless, these data strongly support a model in which TORC1 controls Tco89 proteolysis primarily

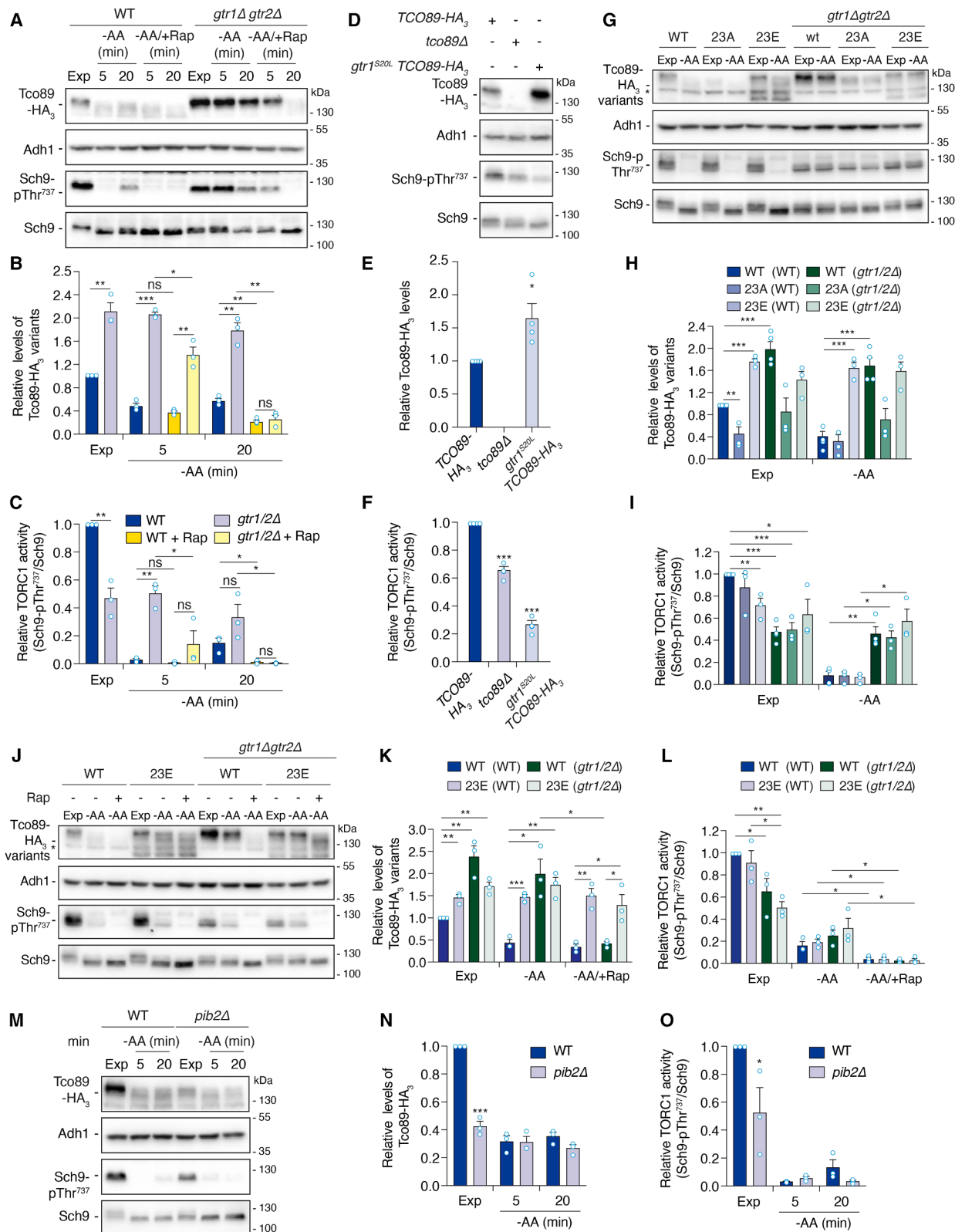
through the phosphorylation of these 23 residues thereby preventing it from being processed by the 20S CP.

We also observed subtle but distinct phenotypes in cells expressing Tco89^{23A}-HA₃ and Tco89^{23E}-HA₃. For example, unlike WT and Tco89^{23E}-HA₃ cells, Tco89^{23A}-HA₃ cells failed to rapidly reestablish pre-starvation Tco89 levels upon glutamine refeeding. This defect was coupled with a transient impairment in Sch9-Thr⁷³⁷ rephosphorylation (Figures 2C–2E). Thus, TORC1-mediated Tco89 phosphorylation and consequent stabilization are critical for the efficient reactivation of TORC1 toward Sch9. Moreover, Tco89^{23E}-HA₃ cells, unlike WT and Tco89^{23A}-HA₃ cells, displayed mildly reduced TORC1 activity, consistent with their moderate rapamycin sensitivity (Figures 2B, 2C, and 2E). Notably, Tco89^{23E}-HA₃-expressing cells also exhibited a more pronounced reduction in TORC1 activity upon prolonged (6 and 24 h) amino acid starvation. During this prolonged starvation, this allele exhibited increased resistance to (presumably autophagy-mediated) degradation compared to WT Tco89 (Figures S2B–S2D). Given that the TORC1-Sch9 branch antagonizes chronological lifespan (CLS),⁵⁷ we assessed CLS in long-term amino-acid-starved batch cultures. Mirroring their reduced TORC1 activity, *tco89^{23E}* cells, but not *tco89^{23A}* cells, displayed a significant increase in CLS compared to WT cells, whereas *TCO89* deletion resulted in an even more pronounced CLS extension (Figures S2E and S2F). We propose that the reduced TORC1 function observed in Tco89^{23E} cells may stem from the unphysiologically high abundance of Tco89^{23E} interfering with the stoichiometric assembly and/or function of the TORC1 complex. This hypothesis is supported by co-immunoprecipitation (coIP) assays demonstrating increased relative association of Tco89^{23E}-HA₃ with GFP-Tor1 compared to the association of Tco89-HA₃ or Tco89^{23A}-HA₃ with GFP-Tor1 (Figures 2F and 2G).

Finally, we examined the subcellular localization of GFP-tagged Tco89^{23A} and Tco89^{23E} using fluorescence microscopy. Both Tco89 alleles localized primarily to the vacuole and were occasionally observed in perivacuolar foci, previously identified as signaling endosomes.^{58,59} However, Tco89^{23E}-GFP exhibited a slightly increased cytoplasmic presence (Figure 2H). Given that *TCO89* deletion results in GFP-Tor1 redistribution from the vacuolar membrane to signaling endosomes,⁵⁸ we investigated the capacity of Tco89^{23A} and Tco89^{23E} to maintain proper GFP-Tor1 localization. In agreement with prior findings, Tco89 loss caused GFP-Tor1 dispersal from the vacuolar membrane and accumulation in signaling endosomes (Figure 2I). This effect was recapitulated, albeit to a lesser extent, in *tco89^{23A}* cells. In contrast, *tco89^{23E}* cells exhibited largely normal vacuolar GFP-Tor1 localization but also displayed elevated levels of GFP-Tor1 foci at endosomes (Figure 2I). In summary, expression of Tco89^{23E}, which bypasses TORC1-mediated Tco89 phosphorylation, negatively impacts TORC1 function, likely due to its accumulation to unphysiologically high levels. However, our data with Tco89^{23A} demonstrate that TORC1-mediated phosphorylation stabilizes Tco89 and thereby also promotes TORC1 localization to vacuolar membranes where it can activate Sch9.

Rag GTPases are required for proteolysis of Tco89

In investigating how Tco89 contributes to TORC1 function, we observed that loss of the Rag GTPases (in a *gtr1Δ gtr2Δ* double



(legend on next page)

mutant), which reduced TORC1 activity (i.e., relative Sch9-pThr⁷³⁷/Sch9 levels) as previously reported,¹⁶ paradoxically increased phosphorylated Tco89 levels (Figures 3A and 3B). This observation is in line with a recent phosphoproteomic analysis of exponentially growing *gtr1Δ gtr2Δ* cells, which revealed significantly elevated phosphorylation of specific Tco89 residues (e.g., Ser⁷⁴) compared to WT cells.⁶⁰ Furthermore, upon amino acid starvation, *gtr1Δ gtr2Δ* cells exhibited a partial defect in complete TORC1 inhibition, consistent with prior findings.^{16,61,62} This partial inhibition correlated with enhanced resistance of Tco89 to degradation (Figures 3A–3C). However, simultaneous amino acid starvation and rapamycin treatment in these cells fully abrogated TORC1 activity and induced Tco89 degradation (Figures 3A and 3B). Given that Rag GTPase loss compromised TORC1-mediated Sch9, but not Tco89, phosphorylation in exponentially growing cells, we examined cells expressing the inactive, nucleotide-free *Gtr1^{S20L}* allele, which, like *Gtr1^{S20N}*,^{16,63} is defective for TORC1 binding. These cells phenocopied *gtr1Δ gtr2Δ* cells, exhibiting reduced relative Sch9-Thr⁷³⁷ phosphorylation but elevated phosphorylated Tco89-HA₃ levels (Figures 3D–3F). These data indicate that the vacuolar Rag GTPases primarily position TORC1 to control Sch9 (and other substrates) phosphorylation and that their loss or inactivation disrupts this localization-dependent mechanism but does not directly inactivate TORC1 per se. Consequently, we predicted that Rag GTPase loss should result in reduced TORC1 activity toward Sch9 in exponentially growing cells, regardless of the Tco89 allele, and have minimal impact on Tco89^{23E}-HA₃ stability and Tco89^{23A}-HA₃ instability. This was indeed the case (Figures 3G–3I). Finally, Tco89^{23E}-HA₃ remained remarkably stable even in *gtr1Δ gtr2Δ* cells subjected to combined amino acid starvation and rapamycin treatment (Figures 3J–3L).

Another presumably allosteric TORC1 regulator acting in parallel to the Rag GTPases is Pib2.⁶⁴ This glutamine and cysteine sensor, via its FYVE domain, associates with phosphatidylinositol-3-phosphate (PI3P) on membranes and exerts both positive and negative control over TORC1 in response to the presence and absence of amino acids, respectively.^{64–71} As expected, loss of Pib2 significantly reduced TORC1 activity toward Sch9 and Tco89, reflected by the low Tco89 levels in exponentially growing *pib2Δ* cells (Figures 3M–3O). In addition, both the low

Sch9 phosphorylation and the low Tco89 levels remained partially sensitive to amino acid starvation, which is likely due to residual Rag GTPase inactivation under these conditions. These observations support a model whereby the Rag GTPases, by correctly positioning Pib2,^{65,72} TORC1, and Sch9, enable Pib2 to regulate TORC1-mediated Sch9 phosphorylation, analogous to the allosteric regulation of mammalian mTORC1 by Rheb. This coordinating role is supported by the documented interaction between Rag GTPases and Pib2 in yeast two-hybrid assays.^{70,73} We independently confirmed and extended these findings using a membrane-bound yeast two-hybrid system. Among the five subunits of the EGO complex (EGOC), Gtr1, Ego2, and Ego3 directly interacted with Pib2 (Figure S3A). Notably, these interactions were abolished upon deletion of any of the other EGOC subunits (Figure S3B), indicating that Pib2 specifically recognizes the intact EGOC complex. This may explain the previous failure of coIP assays to detect these interactions.^{65,70} Furthermore, we found that Gtr1 interacts with Pib2 via its N-terminal nucleotide-binding domain (amino acids 1–184; Figure S3C), suggesting that this interaction is dynamically regulated by the Gtr1 nucleotide status. Consistent with this hypothesis, Pib2 interacted robustly with the GTP-locked *Gtr1^{Q65L}* allele (mimicking the active state) but failed to interact with the inactive, nucleotide-free *Gtr1^{S20L}* allele (Figure S3D), demonstrating that this interaction is favored in the presence of amino acids and active Gtr1. Taken together, these observations provide a compelling mechanistic basis for the previously proposed model of cooperative TORC1 activation by Pib2 and the Rag GTPases upon amino acid stimulation.^{64,72}

The structured C-terminal domain of Tco89 warrants regular TORC1 signaling

Based on the observed synthetic lethality of loss of Tco89 combined with loss of Pib2, mirroring the genetic interaction between loss of Gtr1 and loss of Pib2,⁷⁰ we hypothesized that these three proteins function in concert to tether TORC1 to vacuolar membranes. This hypothesis was supported by coIP analyses demonstrating the association of active, but not inactive, Rag GTPases with the TORC1 subunits Kog1 and Tco89¹⁶ and by two-hybrid assays revealing an interaction between the Tco89 C terminus and Gtr1.⁶³ This C-terminal domain is characterized

Figure 3. Rag GTPases are required for proteolysis of Tco89

- (A) Loss of Rag GTPases boosts Tco89 levels and reduces Tco89 degradation in a TORC1-dependent manner. WT and *gtr1Δ gtr2Δ* cells expressing Tco89-HA₃ were grown exponentially in SC (Exp) and starved (–AA) for amino acids ± 200 nM rapamycin (+Rap). Lysates were analyzed as in Figure 1A.
 - (B and C) Relative levels of Tco89-HA₃ (B) and TORC1 activities (C) quantified from (A) (as in Figures 1B and 1C). Color code in (C).
 - (D) Tco89 levels are enhanced in cells expressing nucleotide-free, inactive *Gtr1^{S20L}*. WT and *gtr1^{S20L}* cells expressing Tco89-HA₃ and *tco89Δ* control cells were grown exponentially and analyzed as in (A).
 - (E and F) Relative Tco89-HA₃ levels (E) and TORC1 activities (F) quantified from (D) (as in Figures 1B and 1C; n = 4).
 - (G) Genetic interactions between *tco89^{23A/E}* and *gtr1Δ gtr2Δ*. WT and *gtr1Δ gtr2Δ* cells expressing Tco89-HA₃ variants were grown exponentially (Exp), starved for amino acids (–AA; 20 min), and analyzed as in (A).
 - (H and I) Relative Tco89-HA₃ variant levels (H) and TORC1 activities (I) quantified from (G) (as in Figures 1B and 1C). Color code in (H).
 - (J) Tco89^{23E} stability in *gtr1Δ gtr2Δ* cells depends on TORC1. Cells were grown, treated, and analyzed as in (G), with rapamycin (+Rap) added during amino acid starvation.
 - (K and L) Relative Tco89-HA₃ variant levels (K) and TORC1 activities (L) quantified from (J) (as in Figures 1B and 1C).
 - (M) Loss of Pib2 causes low TORC1 activity and Tco89 levels. WT and *pib2Δ* cells expressing Tco89-HA₃ were grown exponentially (Exp), starved for amino acids (–AA), and analyzed as in (A). See also Figure S3.
 - (N and O) Relative Tco89-HA₃ levels (N) and TORC1 activities (O) quantified from (M) (as in Figures 1B and 1C).
- Asterisks in (G) and (J): cross-reacting band. *p < 0.05, **p < 0.005, and ***p < 0.0005 (paired Student's t test relative to WT [Exp]).

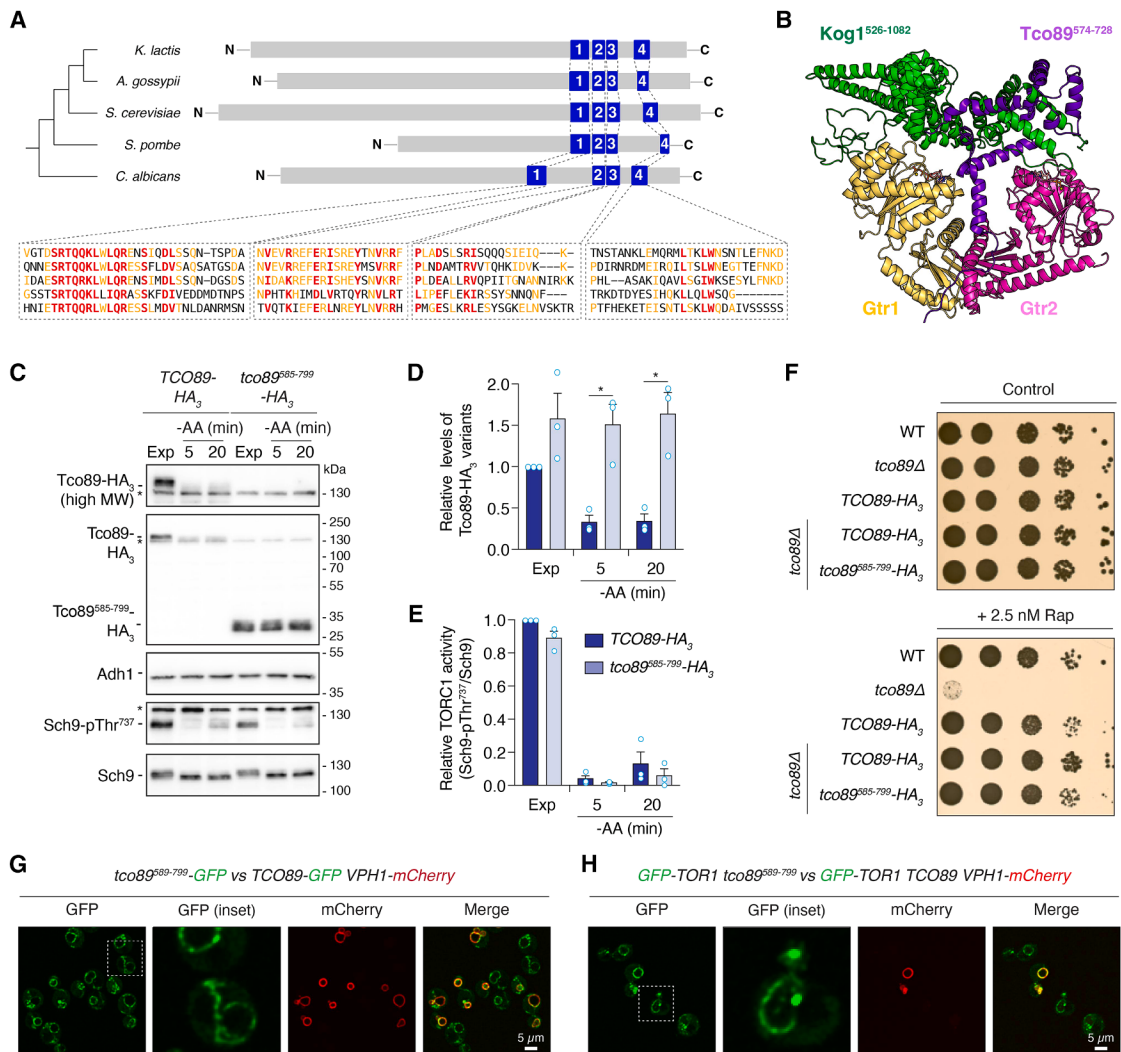


Figure 4. The Tco89 C terminus is sufficient for TORC1 signaling

(A) Alignment of *S. cerevisiae* Tco89 with fungal orthologs (*Kluyveromyces lactis*, *Ashbya gossypii*, *Schizosaccharomyces pombe*, and *Candida albicans*), adjusted to the second of four conserved α helices (blue), with aligned sequences below (conserved residues in bold red or orange, if conserved among only three or four of these species).

(B) AlphaFold prediction of the Tco89 C-terminal domain (residues 574–728, violet) with Gtr1^{GTP} (gold), Gtr2^{GDP} (pink), and a central domain of Kog1 (residues 526–1082, green).

(C) The Tco89 C terminus is functional and hyperstable. Cells expressing Tco89-HA₃ or Tco89^{585–799}-HA₃ were grown exponentially in SC (Exp), starved for amino acids (-AA), and analyzed as in Figure 1A. The top (high MW) shows a better resolution of the slowly migrating Tco89-HA₃. Asterisk: cross-reacting band.

(D and E) Relative Tco89-HA₃ variant levels (D) and TORC1 activities (E) quantified from (C) as in Figures 1B and 1C. Color code in (E). *p < 0.05 (paired Student's t test relative to the indicated reference).

(F) Tco89 C terminus and rapamycin sensitivity. WT and mutants were pre-grown, spotted on plates without (control) or with 2.5 nM rapamycin (+Rap), and grown for 3 days at 30°C as in Figure 2B.

(G) Subcellular localization of Tco89^{585–799}-GFP. Cells were grown exponentially, and the ones expressing Tco89^{585–799}-GFP were mixed with cells co-expressing Tco89-GFP and Vph1-mCherry prior to visualization by confocal fluorescence microscopy. A total of 83% ± 5% of Tco89^{585–799}-GFP-expressing cells showed GFP-Tor1 foci (n = 292) versus 28% ± 8% in WT cells (n = 377). Scale bar: 5 μ m.

(H) GFP-Tor1 localization in mixed cultures of Tco89^{585–799}-expressing and Tco89- and Vph1-mCherry-expressing cells grown and analyzed as in (G).

by four α helices (Figure 4A), while the remaining regions appear predominantly disordered (AlphaFold prediction; AF-Q08921-F1).^{74,75} Notably, sequence alignments and AlphaFold comparisons revealed the conservation of these four α helices in Tco89 orthologs across diverse fungal species (Figure 4A). Within α helix 1, a short stretch of residues (589–707) specifically interacted

with Gtr1, and both Gtr1 and Gtr2 interacted with the central HEAT-repeat-containing domain of Kog1 in yeast two-hybrid assays.⁶³ These findings prompted us to model the interaction between Gtr1, Gtr2, the four Tco89 α helices, and the HEAT repeats of Kog1 using AlphaFold. The resulting model, which remained stable during a 400-ns molecular dynamics (MD) simulation,

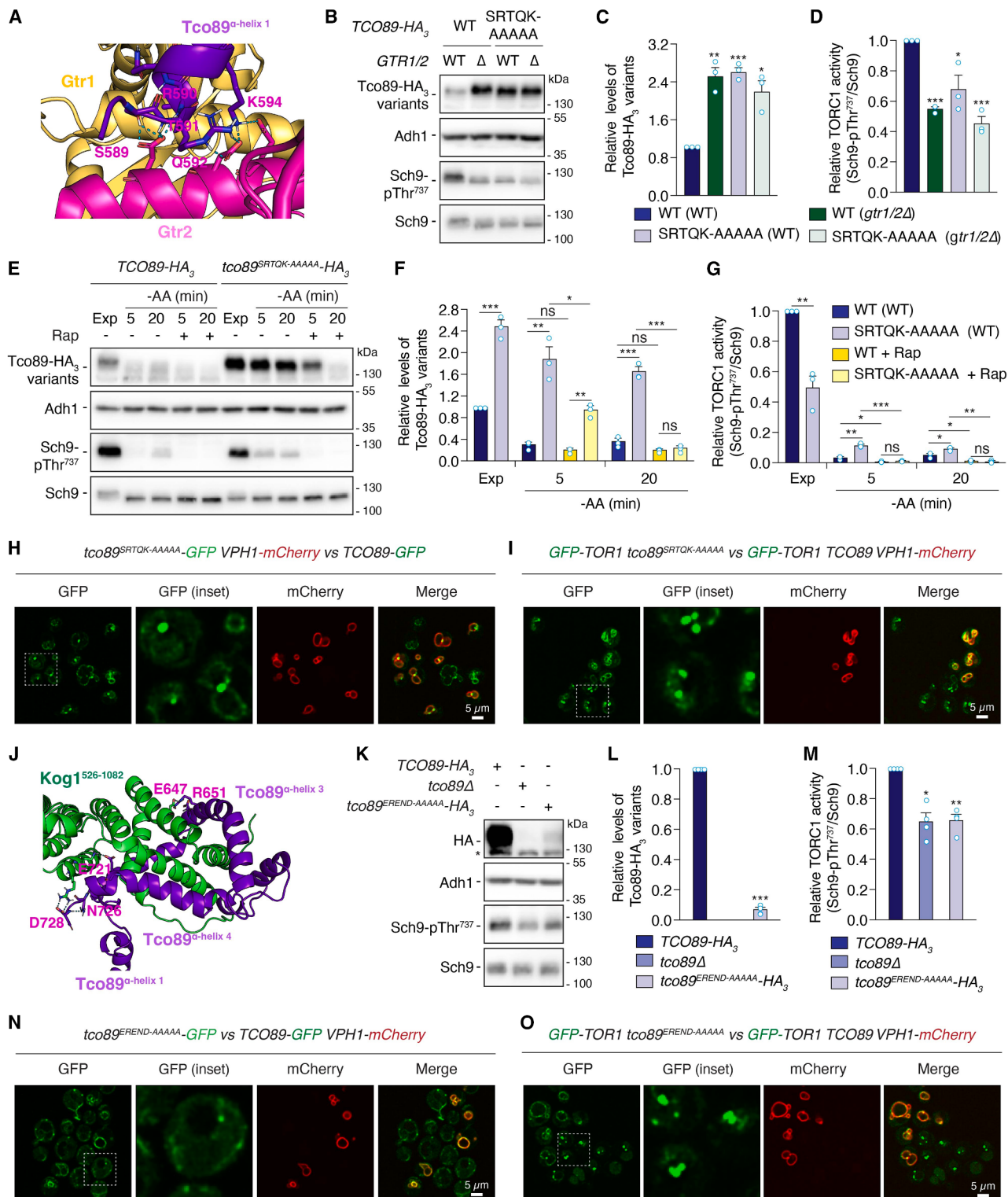


Figure 5. Tco89 functions as an adaptor between the Rag GTPases and Kog1

(A) AlphaFold prediction of Tco89 α helix 1 (violet) with Gtr1 (gold) and Gtr2 (pink). The five residues (Ser⁵⁸⁹, Arg⁵⁹⁰, Thr⁵⁹¹, Gln⁵⁹², and Lys⁵⁹⁴; SRTQK) in Tco89 predicted for Gtr1-Gtr2 hydrogen bonding are highlighted.

(B) Tco89^{SRTQK-AAAAAA} stability in WT and gtr1Δgtr2Δ cells (Δ). Cells expressing TCO89-HA₃ or tco89^{SRTQK-AAAAAA}-HA₃ were grown exponentially in SC (Exp) and lysates were analyzed as in Figure 1A.

(legend continued on next page)

revealed that Tco89 α helix 1 inserts into the cleft between Gtr1 and Gtr2, while the remaining three α helices wrap around a specific Kog1 domain (residues 924–1,023) adjacent to the Gtr1-binding HEAT repeats (Figure 4B). Consistently, the GST-tagged C terminus of Tco89 (residues 585–799) strongly interacted with both the recombinant Gtr1-Gtr2 heterodimer and a truncated Kog1 fragment (residues 536–1,082) encompassing the predicted Gtr1- and Tco89-interaction domain (Figures S4A and S4B).

This Tco89 domain also displayed a weaker interaction with Gtr1 and Gtr2 in a membrane-bound yeast two-hybrid system (Figure S4C). To directly assess the *in vivo* function of this domain, we expressed HA₃-tagged Tco89^{585–799} in *tco89 Δ* cells. Unlike full-length Tco89-HA₃, Tco89^{585–799}-HA₃ remained stable during amino acid starvation (Figures 4C and 4D), indicating that the unstructured Tco89 N terminus is required for proteasomal targeting. Importantly, Tco89^{585–799}-HA₃-expressing cells exhibited only faint rapamycin sensitivity and displayed normal TORC1 activity (toward Sch9) during both exponential growth and amino acid starvation (Figures 4C–4F). Furthermore, GFP-tagged Tco89^{585–799} localized appropriately to vacuolar membranes (Figure 4G). The only mild phenotype observed in Tco89^{585–799}-expressing cells was a partial accumulation of GFP-Tor1 on signaling endosomes, while vacuolar membrane-associated GFP-Tor1 was retained (Figure 4H). Thus, the structured C-terminal domain of Tco89 is sufficient to ensure appropriate TORC1 control.

Tco89 tethers TORC1 to Rag GTPases

To examine the role of Tco89 in mediating Kog1 association with the Rag GTPases (Figure 4B), we generated Tco89 mutations predicted to disrupt these critical interactions. Specifically, we mutated five residues (Ser⁵⁸⁹, Arg⁵⁹⁰, Thr⁵⁹¹, Gln⁵⁹², and Lys⁵⁹⁴; SRTQK) within Tco89 α helix 1, which AlphaFold modeling and MD simulations predicted to form hydrogen bonds with the Rag GTPase cleft (Figure 5A; Table S2). As anticipated, this SRTQK-to-AAAAA mutation within the GST-tagged C-terminal Tco89 domain (Tco89^{585–799,SRTQK-AAAAA}) significantly impaired its binding to recombinant Gtr1-Gtr2 in pull-down assays and partially compromised Tco89^{SRTQK-AAAAA} binding to Gtr1-Gtr2 in two-hybrid assays (Figures S4A and S4C). *In vivo*, expression of full-length Tco89^{SRTQK-AAAAA}-HA₃ phenocopied

Rag GTPase loss, resulting in reduced TORC1 activity (toward Sch9) that was only partially responsive to inhibition following amino acid starvation (Figures 3A–3C and 5B–5D) and conferred rapamycin sensitivity (Figure S4D). This mutation also led to Tco89^{SRTQK-AAAAA} accumulation, with the mutant protein remaining stable even in amino-acid-starved cells, unless these cells were concomitantly treated with rapamycin (Figures 5B, 5C, 5E, and 5F) or the allele was combined with Ser/Thr-to-Ala mutations of the 23 TORC1-sensitive residues (Figures S5A–S5C). In agreement with its impaired Rag GTPase association, GFP-tagged Tco89^{SRTQK-AAAAA} was dispersed from vacuolar membranes and accumulated in signaling endosomes (Figure 5H). Mirroring observations in Tco89-deficient cells,⁵⁹ GFP-Tor1 also redistributed from vacuolar membranes to signaling endosomes in Tco89^{SRTQK-AAAAA}-expressing cells (Figure 5I).

AlphaFold modeling also suggested that Tco89 α helices 2–4 might interact with Kog1. To test this, we mutated five residues (Glu⁶⁴⁷, Arg⁶⁵¹, Glu⁷²¹, Asn⁷²⁶, and Asp⁷²⁸; EREN) predicted to engage in hydrogen bonding with Kog1 (Figure 5J; Table S3). The resulting Tco89^{EREN-AAAAA} allele exhibited a significant defect in Kog1 binding, but not in Gtr1 or Gtr2 binding, in yeast two-hybrid assays (Figure S4C). Strikingly, *tco89^{EREN-AAAAA}-HA₃* cells displayed dramatically reduced levels of the HA₃-tagged protein (Figures 5K and 5L). This observation was anticipated, as Tco89 detachment from Kog1 would be expected to prevent its efficient phosphorylation by TORC1, rendering it highly susceptible to degradation. Consequently, *tco89^{EREN-AAAAA}* cells exhibited low TORC1 activity (toward Sch9) and pronounced rapamycin sensitivity comparable to that of *tco89 Δ* cells (Figures 5K, 5M, and S4D). Mutation of only two of these residues (Glu⁶⁴⁷ and Arg⁶⁵¹), generating the *tco89^{ER-AA}-HA₃* mutant, yielded an intermediate phenotype, with approximately 50% reduction in Tco89^{ER-AA}-HA₃ levels and mild rapamycin sensitivity, but no detectable effect on Sch9-Thr⁷³⁷ phosphorylation or the subcellular localization of either Tco89^{ER-AA}-GFP or GFP-Tor1 (Figures S4D and S5D–S5H). In contrast, Tco89^{EREN-AAAAA}-GFP was barely detectable by fluorescence microscopy (Figure 5N), and GFP-Tor1 almost completely localized to signaling endosomes in *tco89^{EREN-AAAAA}* cells, as observed in *tco89 Δ* cells (Figures 2I and 5O). While Tco89^{EREN-AAAAA} expression could be partially enhanced by combining it with phosphomimetic

(C and D) Relative Tco89-HA₃ variant levels (C) and TORC1 activities (D) quantified from (B) (as in Figures 1B and 1C). See also Figures S4 and S5.

(E) Tco89^{SRTQK-AAAAA}-HA₃ stability depends on TORC1. Tco89-HA₃- and Tco89^{SRTQK-AAAAA}-HA₃-expressing cells were grown exponentially in SC (Exp), amino acid starved (–AA) with (+) or without (–) 200 nM rapamycin (Rap), and analyzed as in Figure 1A.

(F and G) Relative Tco89-HA₃ variant levels (F) and TORC1 activities (G) quantified from (E) (as in Figures 1B and 1C). Color code in (G).

(H) Tco89^{SRTQK-AAAAA}-GFP localization. Cells were grown exponentially, and the ones co-expressing Tco89^{SRTQK-AAAAA}-GFP and Vph1-mCherry were mixed with cells expressing Tco89-GFP prior to visualization (as in Figure 2H; scale bar: 5 μ m).

(I) GFP-Tor1 localization in mixed cultures of *tco89^{SRTQK-AAAAA}* and *TCO89 VPH1-mCherry* cells grown and analyzed as in (H) (scale bar: 5 μ m).

(J) AlphaFold prediction of Tco89 α helices 1–4 (violet) with a central domain of Kog1 (residues 526–1082; green). The five residues (Glu⁶⁴⁷, Arg⁶⁵¹, Glu⁷²¹, Asn⁷²⁶, and Asp⁷²⁸; EREN) in Tco89 predicted for Kog1 hydrogen bonding are highlighted.

(K) Tco89^{EREN-AAAAA} is barely detectable by immunoblot analysis. WT cells expressing Tco89-HA₃ or Tco89^{EREN-AAAAA}-HA₃ and *tco89 Δ* cells were grown and analyzed as in (B).

(L and M) Relative Tco89-HA₃ variant levels (L) and TORC1 activities (M) quantified from (K) ($n = 4$) (as in Figures 1B and 1C).

(N) Tco89^{EREN-AAAAA}-GFP localization. Cells were grown exponentially, and the ones expressing Tco89^{EREN-AAAAA}-GFP were mixed with cells co-expressing Tco89-GFP and Vph1-mCherry prior to visualization as in (H) (scale bar: 5 μ m).

(O) GFP-Tor1 localization in mixed cultures of *tco89^{EREN-AAAAA}* and *TCO89 VPH1-mCherry* cells grown and analyzed as in (H) (scale bar: 5 μ m).

* $p < 0.05$, ** $p < 0.005$, and *** $p < 0.0005$ (paired Student's *t* test, relative to the indicated reference).

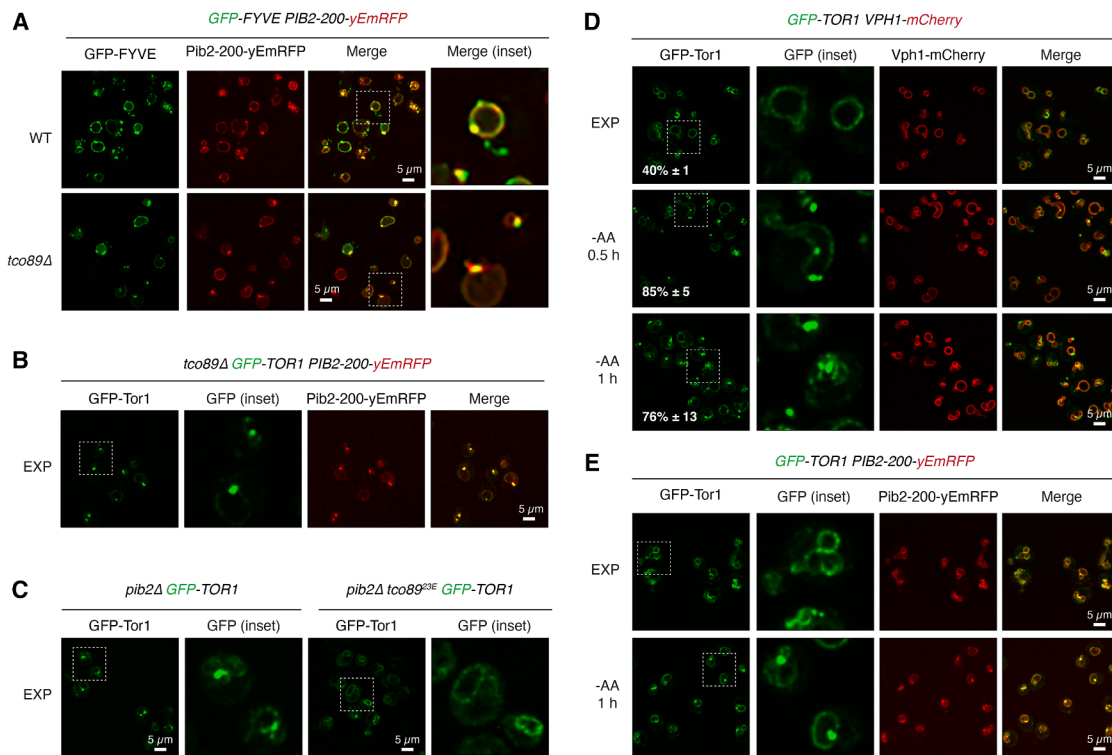


Figure 6. Amino-acid-starvation-induced proteolysis of Tco89 sequesters TORC1 in endosomes

(A) Pib2 co-localizes with GFP-FYVE in signaling endosomes in the absence of Tco89. Exponentially growing WT and *tco89Δ* cells co-expressing GFP-FYVE (of EEA1⁵⁹) and Pib2-200-yEmRFP were visualized as in Figure 2H. See also Figure S6.

(B) Tor1 and Pib2 co-localize on signaling endosomes in the absence of Tco89. Exponentially growing *tco89Δ* cells co-expressing GFP-Tor1 and Pib2-200-yEmRFP were visualized as in Figure 2H.

(C) Expression of Tco89^{23E} prevents accumulation of Tor1 in foci. Exponentially growing *pib2Δ* or *pib2Δ tco89^{23E}* cells expressing GFP-Tor1 were visualized as in Figure 2H. A total of 83% ± 6% of *pib2Δ* cells presented GFP-Tor1 foci ($n = 303$), compared to 30% ± 9% in *pib2Δ tco89^{23E}* cells ($n = 515$).

(D and E) Amino acid starvation shifts Tor1 to Pib2-positive endosomes. Exponentially growing WT cells expressing GFP-Tor1 and either Vph1-mCherry (D) or Pib2-200-yEmRFP (E) were starved for amino acids for the indicated times and visualized as in Figure 2H.

mutations of the 23 TORC1-sensitive residues (Figures S5I–S5K), the resulting Tco89^{23E}-EREND-AAAAA variant still exhibited very low TORC1 activity toward Sch9, underscoring its inability to facilitate Rag GTPase-mediated TORC1 regulation (Figures S5I–S5K). In summary, the structured C-terminal domain of Tco89 functions as a molecular clamp, bringing together TORC1 (via Kog1) and the Rag GTPases on vacuolar membranes, while the unstructured N-terminal region determines the rate of Tco89 degradation in response to TORC1 activity.

Tco89 proteolysis induces spatial separation of TORC1 from vacuolar substrates

Loss of Tco89, like loss of the Rag GTPases, causes GFP-Tor1 redistribution from vacuolar membranes to perivacuolar foci^{59,62,76} termed signaling endosomes.⁵⁸ Consistently, loss of Gtr1 and Gtr2 also resulted in the relocation of Tco89-GFP from vacuolar membranes to yEmRFP-Tor1-positive signaling endosomes, where Tco89 and Tor1 remained associated with each other (Figures S6A and S6B). Interestingly, Pib2-200-yEmRFP, which interacts with Kog1, Rag GTPases (Figure S3), and PI3P via its FYVE domain,^{64,69} was localized to both vacuolar and endosomal membranes in WT cells.^{65,70,72} However,

in exponentially growing *tco89Δ* cells, like in cells lacking Gtr1 (and/or Gtr2),^{65,72} Pib2-200-yEmRFP largely shifted to GFP-FYVE-positive endosomes and also perfectly co-localized with GFP-Tor1 (Figures 6A and 6B). Notably, in *tco89Δ* cells, neither GFP-Gtr1 (Figure S6C) nor mNeonGreen-Sch9 (Figure S6D) accumulated in these foci but remained predominantly at the vacuolar membrane. Thus, loss of Tco89 (1) specifically abolishes Rag GTPase-mediated TORC1 tethering to vacuolar membranes, thereby disrupting its control over vacuolar effectors (e.g., Sch9), and (2) promotes the clustering of both TORC1 and Pib2 on PI3P-rich endosomes in nutrient-rich media, likely driven by the affinity of Pib2 for Kog1 and PI3P. Combined, these data also explain why loss of the Rag GTPases reduces TORC1-mediated phosphorylation of Sch9 while not interfering with continued phosphorylation and stabilization of Tco89 by endosomal Pib2-TORC1 in cells growing on rich nutrients (Figures 3A–3C).

Because Pib2 binds to and controls TORC1 in part via Kog1, its loss expectedly restricts TORC1 activity not only toward Sch9 but also toward Tco89, leading to its degradation when cells are growing under nutrient-rich conditions (Figures 3M–3O). Our data therefore predicted that GFP-Tor1 would

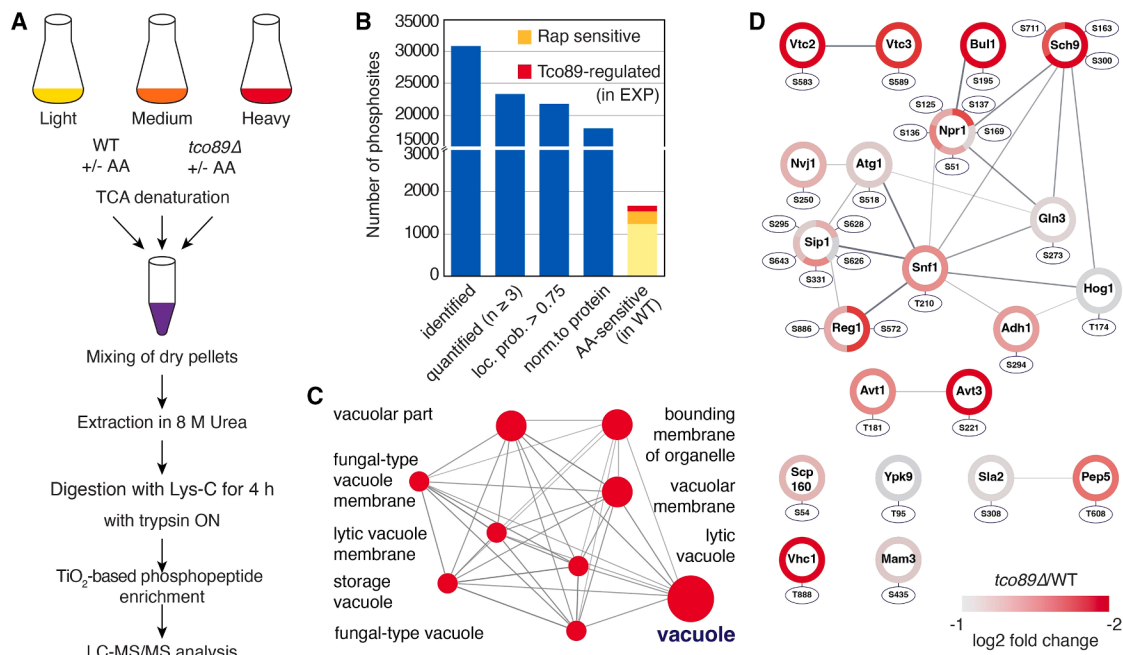


Figure 7. The Tco89-sensitive phosphoproteome

(A) Experimental workflow. WT and *tco89Δ* cells were SILAC (stable isotope labeling by amino acids in cell culture) labeled and processed as outlined. (B) Identified and quantified phosphosites. Data were filtered as indicated. Rapamycin (Rap)-sensitive sites were derived from our published datasets.^{44,77} (C) GO analysis of Tco89-sensitive phosphosites indicates an enrichment of vacuolar target proteins. ($p < 0.05$, Bonferroni step-down corrected). (D) Protein interaction network of vacuolar target proteins that carry significantly regulated, Tco89-sensitive phosphosites ($p < 0.05$ and minimum 2-fold regulated).

also primarily localize to signaling endosomes and be depleted from vacuolar membranes in *pib2Δ* cells. This was indeed the case (Figure 6C), in agreement with a previous report.⁷² Remarkably, expression of the stable Tco89^{23E} variant restored GFP-Tor1 localization to the vacuole in *pib2Δ* cells (Figure 6C). This observation demonstrates that GFP-Tor1 localization to vacuolar membranes requires both the Rag-GTPase-Tco89 module and Pib2. Because amino acid starvation inactivates Rag GTPases, disrupts their association with Pib2, and induces Tco89 proteolysis, we expected TORC1 to redistribute from vacuolar membranes and accumulate at endosomes in amino-acid-starved cells. As predicted and previously demonstrated,^{62,76} a significant fraction of GFP-Tor1 indeed redistributed from vacuolar membranes to signaling endosomes upon amino acid starvation, co-localizing with Pib2-200-yEmRFP (Figures 6D and 6E).

The Tco89-sensitive phosphoproteome

To confirm that Tco89 loss specifically compromises vacuolar TORC1 function, we performed quantitative phosphoproteomics comparing WT and *tco89Δ* cells both in the presence of and after starvation for amino acids (Figure 7A; $n = 3$ biological replicates each). Following data processing and filtering, we quantified 17,917 phosphosites localized to specific amino acid residues and normalized to their respective target proteins (Figure 7B; Table S4A). Of these, 1,757 sites exhibited amino-acid-starvation-sensitive phosphorylation in WT cells ($p < 0.05$, fold change ≥ 2). Filtering this subset for known TORC1-regulated, rapamy-

cin-sensitive phosphosites (using previously published datasets^{44,77}) identified 415 sites, of which 123 (27%) also displayed altered phosphorylation in response to Tco89 loss in exponentially growing cells (Table S4B). As expected, the vast majority (98%) of these sites showed no differential regulation in amino-acid-starved WT and amino-acid-starved *tco89Δ* cells, indicating that Tco89 specifically impacts TORC1 signaling under nutrient-rich conditions. Gene Ontology (GO) enrichment analysis of the proteins containing these Tco89-sensitive phosphosites revealed a significant enrichment for vacuolar proteins (Figure 7C). Remarkably, 21 vacuolar proteins harbored between one and five significantly regulated, Tco89-sensitive phosphosites (Figure 7D). This group included Sch9 (with the well-established TORC1 target Ser⁷¹¹),⁴⁶ as anticipated, as well as other vacuolar membrane-associated proteins, such as the vacuolar transporter chaperone (VTC) complex subunits Vtc2 and Vtc3⁷⁸; the vacuolar amino acid permeases Avt1 and Avt3⁷⁹; the vacuolar polyamine, cation-chloride, and Mg²⁺ transporters Ypk9, Mam3, and Vhc1,^{80–82} respectively; and both the catalytic α subunit of the Snf1 kinase and its regulatory β subunit Sip1 (which targets the SNF1/AMPK complex to the vacuolar membrane).⁸³ These findings significantly expand our understanding of the role of Tco89 in regulating vacuolar TORC1 signaling. We reasoned that the remaining 292 (65%) rapamycin- and amino-acid-sensitive phosphosites that were not sensitive to Tco89 loss might be targeted by TORC1 at distinct subcellular locations, such as the signaling endosome. Consistent with this notion, we identified six phosphosites within the previously

characterized endosomal TORC1 substrate Atg13 among these hits.^{44,59} Finally, Pib2 phosphorylation (at eight residues) was significantly responsive to both rapamycin treatment and amino acid starvation, in agreement with the established feedback regulation of Pib2 by TORC1.^{70,84,85} Importantly, Tco89 loss did not significantly affect the phosphorylation of these Pib2 residues, which is also in line with our observation that Pib2 relocates with TORC1 to endosomes in the absence of Tco89 (Figure 6B).

DISCUSSION

Amino acid starvation induces a switch in the Rag GTPase heterodimer from the active Gtr1^{GTP}-Gtr2^{GDP} state to the inactive Gtr1^{GDP}-Gtr2^{GTP} state.^{11,42} However, the mechanistic link between this switch and the differential phosphorylation of TORC1 effectors in yeast has remained unclear.⁸⁶ Our findings reveal that active Rag GTPases, through their interaction with Tco89, position TORC1 on vacuolar membranes, enabling appropriate regulation by Pib2. This membrane localization facilitates access to substrates such as Sch9, which is anchored to the vacuolar membrane via its N-terminal phosphatidylinositol 3,5-bisphosphate (PI(3,5)P₂) binding domain.^{87–89} Upon amino acid starvation, Pib2-mediated TORC1 activation is abrogated (or Pib2-mediated inactivation is favored),^{64,66,72} leading to Tco89 hypophosphorylation and subsequent degradation. This degradation allows SEACIT to promote the inactive state of the Rag GTPases. Critically, in this inactive configuration, the Rag GTPases are unable to interact with Tco89,¹⁶ explaining the requirement for their reactivation to engage newly synthesized Tco89 upon amino acid replenishment. This model elegantly resolves the long-standing question of whether Pib2 and the Rag GTPases function cooperatively or in parallel.⁶⁴ We propose that the Rag GTPases establish a membrane-bound TORC1 configuration that is essential for Pib2-dependent regulation and efficient interaction with downstream effectors. This mechanism parallels the mammalian canonical TORC1 pathway, where Rheb acts as an allosteric regulator of membrane-anchored Rag GTPase-mTORC1.^{26,27} However, Pib2 exhibits a more complex function, capable of mediating substrate-specific TORC1 phosphorylation, like mammalian (and potentially yeast) Rag GTPases.^{60,66,90}

In mammals, the Kog1 ortholog Raptor possesses a “Raptor claw” domain that spans the inter-Rag space, directly associating with the Rag heterodimer when RagC (or RagD) is GDP bound.²⁷ Notably, this domain is absent in yeast Kog1. Our data demonstrate that Tco89 fulfills an analogous function in yeast, but with a key difference: TORC1 directly controls Tco89 levels, thereby coupling cellular amino acid availability with TORC1 spatial distribution. Consistent with previous observations,^{62,76} Tco89 degradation in amino-acid-starved cells is accompanied by a marked redistribution of TORC1 to signaling endosomes. This spatial segregation effectively separates TORC1 from its vacuolar effector and key growth regulator Sch9. However, TORC1 remains present on signaling endosomes, where it is likely poised to inactivate Atg13 upon nutrient repletion.^{58,59} These coordinated processes expectedly contribute to cellular energy conservation under the fluctuating

nutrient conditions encountered by fungi. Finally, despite distinct mechanistic underpinnings, mTORC1 has recently also been shown to autoregulate its lysosomal residence,^{91,92} implying that mTORC1 regulates its effectors in spatially separated pools.⁹³ This dynamic control of subcellular localization through autoregulation may therefore represent a conserved eukaryotic strategy for modulating TORC1 signaling.

Limitations of the study

The precise mechanism by which TORC1 relocates from the vacuolar membrane to associate with signaling endosomes in the absence of Tco89, Rag GTPases, or Pib2, or upon amino acid starvation, remains incompletely understood. We propose that this relocation may be driven by alterations in the distribution of PI3P, PI(3,5)P₂, and potentially other phosphoinositides (PIPs) between vacuolar and endosomal membranes. Crucially, these alterations are regulated by TORC1 itself, which facilitates the conversion of PI3P to PI(3,5)P₂ through the phosphorylation of Fab1, the PI3P 5-kinase.⁸⁷ Notably, Kog1, similar to mammalian Raptor, exhibits preferential binding to PI3P and PI(3,5)P₂, which facilitates its membrane association.^{89,94} Kog1 contains a WD40 domain that shares structural homology with the seven-bladed β propellers of PROPPINs (phosphoinositide-binding β propellers), which interact with PIPs through blades 5 and 6.⁹⁵ We have initiated an analysis of blades 5 and 6 within the WD40 domain of Kog1, which are presumed to associate with PIPs. However, any attempts to mutate this region have rendered Kog1 non-functional, resulting in inviable mutants. Therefore, elucidating both the structural basis of TORC1 and enrichment on signaling endosomes, which may also contribute to the assembly of TORC1 into inactive higher-order condensates,^{96–98} and the corresponding molecular mechanisms will be critical areas for future research.

RESOURCE AVAILABILITY

Lead contact

Requests for further information and resources and reagents should be directed to and will be fulfilled by the lead contact, Claudio De Virgilio (claudio.devirgilio@unifr.ch).

Materials availability

All unique/stable reagents generated in this study are available from the [lead contact](#).

Data and code availability

- Source data for gel images and graphs can be found in Mendeley Data: <https://doi.org/10.17632/nbc2yff7w8.1>.
- Proteomics data are freely available via the PRIDE repository: <https://www.ebi.ac.uk/pride/>; data identifier PRIDE: [PXD059088](https://www.ebi.ac.uk/pride/study/PXD059088).
- This study did not produce any original code.
- Any additional information required to reanalyze the data reported in this paper is available from the [lead contact](#) upon request.

ACKNOWLEDGMENTS

We thank Susanne Stumpf for technical assistance, Takeshi Noda for plasmids, and Christian Ungermaier for critically reading the manuscript. This work was supported by the Canton of Fribourg (to C.D.V. and J.D.), the Swiss National Science Foundation (184671/214824 to C.D.V., 212187 to J.D., and

229588 to C.D.V. and J.D.), the BBSRC (BB/V016334/1 and BB/X018229/1 to R.H.), and the University of Milano-Bicocca (2023-ATE-0068 to F.T.).

AUTHOR CONTRIBUTIONS

Conceptualization, R.N. and C.D.V.; methodology, R.N., M.-P.P.-G., M.C., J. A., M.J., B.P., K.M., F.T., L.D., M.B., M.S., and R.H.; formal analysis, R.N., M.-P.P.-G., M.C., J.A., M.J., F.T., R.H., and J.D.; writing – original draft, R.N. and C.D.V.; writing – review & editing, R.N., M.-P.P.-G., J.D., and C.D.V.; visualization, R.N., M.-P.P.-G., M.C., J.A., and C.D.V.; funding acquisition, C.D.V.

DECLARATION OF INTERESTS

The authors declare no competing interests.

DECLARATION OF GENERATIVE AI AND AI-ASSISTED TECHNOLOGIES IN THE WRITING PROCESS

During the preparation of the revision of this work, the authors used Gemini 2.0 to improve the clarity and conciseness of the text. After using this tool, the authors reviewed and edited the content as needed and take full responsibility for the content of the published article.

STAR★METHODS

Detailed methods are provided in the online version of this paper and include the following:

- KEY RESOURCES TABLE
- EXPERIMENTAL MODEL AND SUBJECT DETAILS
- METHOD DETAILS
 - Yeast strains, plasmids, and growth conditions
 - Denaturing protein extraction and SDS-PAGE
 - Drop spot assays on solid media
 - Co-immunoprecipitation and SDS-PAGE
 - GST pulldown assays
 - Split-ubiquitin yeast two-hybrid assay
 - *In vitro* phosphatase assay
 - Fluorescence microscopy
 - Computational modeling
 - Molecular dynamics simulations
 - Computational analyses
 - Chronological lifespan experiments (CLS)
 - RNA extraction and qRT-PCR
 - TORC1 purification and kinase assay
 - MS sample preparation, phosphopeptide enrichment, and LC-MS/MS analyses
- QUANTIFICATION AND STATISTICAL ANALYSES

SUPPLEMENTAL INFORMATION

Supplemental information can be found online at <https://doi.org/10.1016/j.celrep.2025.115683>.

Received: October 1, 2024

Revised: February 17, 2025

Accepted: April 17, 2025

Published: May 12, 2025

REFERENCES

1. González, A., and Hall, M.N. (2017). Nutrient sensing and TOR signaling in yeast and mammals. *EMBO J.* 36, 397–408. <https://doi.org/10.15252/embj.201696010>
2. Cornu, M., Albert, V., and Hall, M.N. (2013). mTOR in aging, metabolism, and cancer. *Curr. Opin. Genet. Dev.* 23, 53–62. <https://doi.org/10.1016/j.gde.2012.12.005>
3. Liu, G.Y., and Sabatini, D.M. (2020). mTOR at the nexus of nutrition, growth, ageing and disease. *Nat. Rev. Mol. Cell Biol.* 21, 183–203. <https://doi.org/10.1038/s41580-019-0199-y>
4. Wullschleger, S., Loewith, R., and Hall, M.N. (2006). TOR signaling in growth and metabolism. *Cell* 124, 471–484. <https://doi.org/10.1016/j.cell.2006.01.016>
5. Peterson, T.R., Laplante, M., Thoreen, C.C., Sancak, Y., Kang, S.A., Kuehl, W.M., Gray, N.S., and Sabatini, D.M. (2009). DEPTOR is an mTOR inhibitor frequently overexpressed in multiple myeloma cells and required for their survival. *Cell* 137, 873–886. <https://doi.org/10.1016/j.cell.2009.03.046>
6. Sancak, Y., Thoreen, C.C., Peterson, T.R., Lindquist, R.A., Kang, S.A., Spooner, E., Carr, S.A., and Sabatini, D.M. (2007). PRAS40 is an insulin-regulated inhibitor of the mTORC1 protein kinase. *Mol. Cell* 25, 903–915. <https://doi.org/10.1016/j.molcel.2007.03.003>
7. Holst, B., Lunde, C., Lages, F., Oliveira, R., Lucas, C., and Kielland-Brandt, M.C. (2000). *GUP1* and its close homologue *GUP2*, encoding multimembrane-spanning proteins involved in active glycerol uptake in *Saccharomyces cerevisiae*. *Mol. Microbiol.* 37, 108–124. <https://doi.org/10.1046/j.1365-2958.2000.01968.x>
8. Reinke, A., Anderson, S., McCaffery, J.M., Yates, J., 3rd, Aronova, S., Chu, S., Fairclough, S., Iverson, C., Wedaman, K.P., and Powers, T. (2004). TOR complex 1 includes a novel component, Tco89p (YPL180w), and cooperates with Ssd1p to maintain cellular integrity in *Saccharomyces cerevisiae*. *J. Biol. Chem.* 279, 14752–14762. <https://doi.org/10.1074/jbc.M313062200>
9. Brown, C.R., Hung, G.C., Dunton, D., and Chiang, H.L. (2010). The TOR complex 1 is distributed in endosomes and in retrograde vesicles that form from the vacuole membrane and plays an important role in the vacuole import and degradation pathway. *J. Biol. Chem.* 285, 23359–23370. <https://doi.org/10.1074/jbc.M109.075143>
10. Yan, Y., and Kang, B. (2010). Regulation of Vid-dependent degradation of FBPase by TC089, a component of TOR Complex 1. *Int. J. Biol. Sci.* 6, 361–370. <https://doi.org/10.7150/ijbs.6.361>
11. Nicastro, R., Sardu, A., Panchaud, N., and De Virgilio, C. (2017). The architecture of the Rag GTPase signaling network. *Biomolecules* 7, 48. <https://doi.org/10.3390/biom7030048>
12. Bar-Peled, L., and Sabatini, D.M. (2014). Regulation of mTORC1 by amino acids. *Trends Cell Biol.* 24, 400–406. <https://doi.org/10.1016/j.tcb.2014.03.003>
13. Bar-Peled, L., Schweitzer, L.D., Zoncu, R., and Sabatini, D.M. (2012). Ragulator is a GEF for the Rag GTPases that signal amino acid levels to mTORC1. *Cell* 150, 1196–1208. <https://doi.org/10.1016/j.cell.2012.07.032>
14. Dubouloz, F., Deloche, O., Wanke, V., Cameroni, E., and De Virgilio, C. (2005). The TOR and EGO protein complexes orchestrate microautophagy in yeast. *Mol. Cell* 19, 15–26. <https://doi.org/10.1016/j.molcel.2005.05.020>
15. Powis, K., Zhang, T., Panchaud, N., Wang, R., De Virgilio, C., and Ding, J. (2015). Crystal structure of the Ego1-Ego2-Ego3 complex and its role in promoting Rag GTPase-dependent TORC1 signaling. *Cell Res.* 25, 1043–1059. <https://doi.org/10.1038/cr.2015.86>
16. Binda, M., Péli-Gulli, M.P., Bonfils, G., Panchaud, N., Urban, J., Sturgill, T.W., Loewith, R., and De Virgilio, C. (2009). The Vam6 GEF controls TORC1 by activating the EGO complex. *Mol. Cell* 35, 563–573. <https://doi.org/10.1016/j.molcel.2009.06.033>
17. Sancak, Y., Bar-Peled, L., Zoncu, R., Markhard, A.L., Nada, S., and Sabatini, D.M. (2010). Ragulator-Rag complex targets mTORC1 to the lysosomal surface and is necessary for its activation by amino acids. *Cell* 141, 290–303. <https://doi.org/10.1016/j.cell.2010.02.024>

18. Bar-Peled, L., Chantranupong, L., Cherniack, A.D., Chen, W.W., Ottina, K.A., Grabiner, B.C., Spear, E.D., Carter, S.L., Meyerson, M., and Sabatini, D.M. (2013). A Tumor suppressor complex with GAP activity for the Rag GTPases that signal amino acid sufficiency to mTORC1. *Science* 340, 1100–1106. <https://doi.org/10.1126/science.1232044>.
19. Panchaud, N., Péli-Gulli, M.P., and De Virgilio, C. (2013). Amino acid deprivation inhibits TORC1 through a GTPase-activating protein complex for the Rag family GTPase Gtr1. *Sci. Signal.* 6, ra42. <https://doi.org/10.1126/scisignal.2004112>.
20. Panchaud, N., Péli-Gulli, M.P., and De Virgilio, C. (2013). SEACing the GAP that nEGOCiates TORC1 activation: evolutionary conservation of Rag GTPase regulation. *Cell Cycle* 12, 2948–2952. <https://doi.org/10.4161/cc.26000>.
21. Tsun, Z.Y., Bar-Peled, L., Chantranupong, L., Zoncu, R., Wang, T., Kim, C., Spooner, E., and Sabatini, D.M. (2013). The folliculin tumor suppressor is a GAP for the RagC/D GTPases that signal amino acid levels to mTORC1. *Mol. Cell* 52, 495–505. <https://doi.org/10.1016/j.molcel.2013.09.016>.
22. Petit, C.S., Roczniai-Ferguson, A., and Ferguson, S.M. (2013). Recruitment of folliculin to lysosomes supports the amino acid-dependent activation of Rag GTPases. *J. Cell Biol.* 202, 1107–1122. <https://doi.org/10.1083/jcb.201307084>.
23. Péli-Gulli, M.P., Sardu, A., Panchaud, N., Raucci, S., and De Virgilio, C. (2015). Amino acids stimulate TORC1 through Lst4-Lst7, a GTPase-activating protein complex for the Rag family GTPase Gtr2. *Cell Rep.* 13, 1–7. <https://doi.org/10.1016/j.celrep.2015.08.059>.
24. Shen, K., Choe, A., and Sabatini, D.M. (2017). Intersubunit crosstalk in the Rag GTPase heterodimer enables mTORC1 to respond rapidly to amino acid availability. *Mol. Cell* 68, 552–565.e8. <https://doi.org/10.1016/j.molcel.2017.09.026>.
25. Tafur, L., Hinterndorfer, K., Gabus, C., Lamanna, C., Bergmann, A., Sadian, Y., Hamdi, F., Kyriakis, F.L., Kastritis, P.L., and Loewith, R. (2022). Cryo-EM structure of the SEA complex. *Nature* 611, 399–404. <https://doi.org/10.1038/s41586-022-05370-0>.
26. Anandapadamanabhan, M., Masson, G.R., Perisic, O., Berndt, A., Kaufman, J., Johnson, C.M., Santhanam, B., Rogala, K.B., Sabatini, D.M., and Williams, R.L. (2019). Architecture of human Rag GTPase heterodimers and their complex with mTORC1. *Science* 366, 203–210. <https://doi.org/10.1126/science.aax3939>.
27. Rogala, K.B., Gu, X., Kedir, J.F., Abu-Remaihah, M., Bianchi, L.F., Bottino, A.M.S., Dueholm, R., Niehaus, A., Overwijn, D., Fils, A.C.P., et al. (2019). Structural basis for the docking of mTORC1 on the lysosomal surface. *Science* 366, 468–475. <https://doi.org/10.1126/science.aay0166>.
28. Buerger, C., DeVries, B., and Stambolic, V. (2006). Localization of Rheb to the endomembrane is critical for its signaling function. *Biochem. Biophys. Res. Commun.* 344, 869–880. <https://doi.org/10.1016/j.bbrc.2006.03.220>.
29. Long, X., Lin, Y., Ortiz-Vega, S., Yonezawa, K., and Avruch, J. (2005). Rheb binds and regulates the mTOR kinase. *Curr. Biol.* 15, 702–713. <https://doi.org/10.1016/j.cub.2005.02.053>.
30. Yang, H., Jiang, X., Li, B., Yang, H.J., Miller, M., Yang, A., Dhar, A., and Pavletich, N.P. (2017). Mechanisms of mTORC1 activation by RHEB and inhibition by PRAS40. *Nature* 552, 368–373. <https://doi.org/10.1038/nature25023>.
31. Schalm, S.S., Fingar, D.C., Sabatini, D.M., and Blenis, J. (2003). TOS motif-mediated Raptor binding regulates 4E-BP1 multisite phosphorylation and function. *Curr. Biol.* 13, 797–806. [https://doi.org/10.1016/s0960-9822\(03\)00329-4](https://doi.org/10.1016/s0960-9822(03)00329-4).
32. Nojima, H., Tokunaga, C., Eguchi, S., Oshiro, N., Hidayat, S., Yoshino, K. i., Hara, K., Tanaka, N., Avruch, J., and Yonezawa, K. (2003). The mammalian target of rapamycin (mTOR) partner, raptor, binds the mTOR substrates p70 S6 kinase and 4E-BP1 through their TOR signaling (TOS) motif. *J. Biol. Chem.* 278, 15461–15464. <https://doi.org/10.1074/jbc.C200665200>.
33. Dibble, C.C., Elis, W., Menon, S., Qin, W., Klekota, J., Asara, J.M., Finan, P.M., Kwiatkowski, D.J., Murphy, L.O., and Manning, B.D. (2012). TBC1D7 is a third subunit of the TSC1-TSC2 complex upstream of mTORC1. *Mol. Cell* 47, 535–546. <https://doi.org/10.1016/j.molcel.2012.06.009>.
34. Inoki, K., Li, Y., Xu, T., and Guan, K.L. (2003). Rheb GTPase is a direct target of TSC2 GAP activity and regulates mTOR signaling. *Genes Dev.* 17, 1829–1834. <https://doi.org/10.1101/gad.1110003>.
35. Tee, A.R., Manning, B.D., Roux, P.P., Cantley, L.C., and Blenis, J. (2003). Tuberous sclerosis complex gene products, Tuberin and Hamartin, control mTOR signaling by acting as a GTPase-activating protein complex toward Rheb. *Curr. Biol.* 13, 1259–1268. [https://doi.org/10.1016/s0960-9822\(03\)00506-2](https://doi.org/10.1016/s0960-9822(03)00506-2).
36. Demetriades, C., Doumpas, N., and Teleman, A.A. (2014). Regulation of TORC1 in response to amino acid starvation via lysosomal recruitment of TSC2. *Cell* 156, 786–799. <https://doi.org/10.1016/j.cell.2014.01.024>.
37. Settembre, C., Zoncu, R., Medina, D.L., Vetrini, F., Erdin, S., Erdin, S., Huynh, T., Ferron, M., Karsenty, G., Vellard, M.C., et al. (2012). A lysosome-to-nucleus signalling mechanism senses and regulates the lysosome via mTOR and TFEB. *EMBO J.* 31, 1095–1108. <https://doi.org/10.1038/emboj.2012.32>.
38. Settembre, C., Di Malta, C., Polito, V.A., Garcia Arencibia, M., Vetrini, F., Erdin, S., Erdin, S.U., Huynh, T., Medina, D., Colella, P., et al. (2011). TFEB links autophagy to lysosomal biogenesis. *Science* 332, 1429–1433. <https://doi.org/10.1126/science.1204592>.
39. Amick, J., Roczniai-Ferguson, A., and Ferguson, S.M. (2016). C9orf72 binds SMCR8, localizes to lysosomes, and regulates mTORC1 signaling. *Mol. Biol. Cell* 27, 3040–3051. <https://doi.org/10.1091/mbc.E16-01-0003>.
40. Roczniai-Ferguson, A., Petit, C.S., Froehlich, F., Qian, S., Ky, J., Angarola, B., Walther, T.C., and Ferguson, S.M. (2012). The transcription factor TFEB links mTORC1 signaling to transcriptional control of lysosome homeostasis. *Sci. Signal.* 5, ra42. <https://doi.org/10.1126/scisignal.2002790>.
41. Martina, J.A., Chen, Y., Gucek, M., and Puertollano, R. (2012). MTORC1 functions as a transcriptional regulator of autophagy by preventing nuclear transport of TFEB. *Autophagy* 8, 903–914. <https://doi.org/10.4161/auto.19653>.
42. Powis, K., and De Virgilio, C. (2016). Conserved regulators of Rag GTPases orchestrate amino acid-dependent TORC1 signaling. *Cell Discov.* 2, 15049. <https://doi.org/10.1038/celldisc.2015.49>.
43. Caligaris, M., Sampaio-Marques, B., Hatakeyama, R., Pillet, B., Ludovic, P., De Virgilio, C., Winderickx, J., and Nicastro, R. (2023). The yeast protein kinase Sch9 functions as a central nutrient-responsive hub that calibrates metabolic and stress-related responses. *J. Fungi* 9, 787. <https://doi.org/10.3390/jof9080787>.
44. Hu, Z., Raucci, S., Jaquenoud, M., Hatakeyama, R., Stumpe, M., Rohr, R., Reggiori, F., De Virgilio, C., and Dengjel, J. (2019). Multilayered control of protein turnover by TORC1 and Atg1. *Cell Rep.* 28, 3486–3496.e6. <https://doi.org/10.1016/j.celrep.2019.08.069>.
45. Nicastro, R., Brohé, L., Alba, J., Nüchel, J., Figlia, G., Kipschull, S., Gollwitzer, P., Romero-Pozuelo, J., Fernandes, S.A., Lamprakis, A., et al. (2023). Malonyl-CoA is a conserved endogenous ATP-competitive mTORC1 inhibitor. *Nat. Cell Biol.* 25, 1303–1318. <https://doi.org/10.1038/s41556-023-01198-6>.
46. Urban, J., Soulard, A., Huber, A., Lippman, S., Mukhopadhyay, D., Deloche, O., Wanke, V., Anrather, D., Ammerer, G., Riezman, H., et al. (2007). Sch9 is a major target of TORC1 in *Saccharomyces cerevisiae*. *Mol. Cell* 26, 663–674. <https://doi.org/10.1016/j.molcel.2007.04.020>.
47. Caligaris, M., and De Virgilio, C. (2024). Proxies introduce bias in decoding TORC1 activity. *MicroPubl. Biol.* 2024, 001170. <https://doi.org/10.17912/micropub.biology.001170>.
48. Hofer, S.J., Daskalaki, I., Bergmann, M., Friščić, J., Zimmermann, A., Müller, M.I., Abdellatif, M., Nicastro, R., Masser, S., Durand, S., et al.

- (2024). Spermidine is essential for fasting-mediated autophagy and longevity. *Nat. Cell Biol.* 26, 1571–1584. <https://doi.org/10.1038/s41556-024-01468-x>.
49. Shekhar-Guturja, T., Gunaherath, G.M.K.B., Wijeratne, E.M.K., Lambert, J.P., Averette, A.F., Lee, S.C., Kim, T., Bahn, Y.S., Tripodi, F., Ammar, R., et al. (2016). Dual action antifungal small molecule modulates multidrug efflux and TOR signaling. *Nat. Chem. Biol.* 12, 867–875. <https://doi.org/10.1038/nchembio.2165>.
 50. Mizushima, N., Yoshimori, T., and Ohsumi, Y. (2011). The role of Atg proteins in autophagosome formation. *Annu. Rev. Cell Dev. Biol.* 27, 107–132. <https://doi.org/10.1146/annurev-cellbio-092910-154005>.
 51. Lynch-Day, M.A., and Klionsky, D.J. (2010). The Cvt pathway as a model for selective autophagy. *FEBS Lett.* 584, 1359–1366. <https://doi.org/10.1016/febslet.2010.02.013>.
 52. Li, M., Rong, Y., Chuang, Y.S., Peng, D., and Emr, S.D. (2015). Ubiquitin-dependent lysosomal membrane protein sorting and degradation. *Mol. Cell* 57, 467–478. <https://doi.org/10.1016/j.molcel.2014.12.012>.
 53. Lee, D.H., and Goldberg, A.L. (1996). Selective inhibitors of the proteasome-dependent and vacuolar pathways of protein degradation in *Saccharomyces cerevisiae*. *J. Biol. Chem.* 271, 27280–27284. <https://doi.org/10.1074/jbc.271.44.27280>.
 54. Fleming, J.A., Lightcap, E.S., Sadis, S., Thoroddsen, V., Bulawa, C.E., and Blackman, R.K. (2002). Complementary whole-genome technologies reveal the cellular response to proteasome inhibition by PS-341. *Proc. Natl. Acad. Sci. USA* 99, 1461–1466. <https://doi.org/10.1073/pnas.032516399>.
 55. Ben-Nissan, G., and Sharon, M. (2014). Regulating the 20S proteasome ubiquitin-independent degradation pathway. *Biomolecules* 4, 862–884. <https://doi.org/10.3390/biom4030862>.
 56. Suskiewicz, M.J., Sussman, J.L., Silman, I., and Shaul, Y. (2011). Context-dependent resistance to proteolysis of intrinsically disordered proteins. *Protein Sci.* 20, 1285–1297. <https://doi.org/10.1002/pro.657>.
 57. Deprez, M.A., Eskes, E., Winderickx, J., and Wilms, T. (2018). The TORC1-Sch9 pathway as a crucial mediator of chronological lifespan in the yeast *Saccharomyces cerevisiae*. *FEMS Yeast Res.* 18. <https://doi.org/10.1093/femsyr/foy048>.
 58. Hatakeyama, R., and De Virgilio, C. (2019). A spatially and functionally distinct pool of TORC1 defines signaling endosomes in yeast. *Autophagy* 15, 915–916. <https://doi.org/10.1080/15548627.2019.1580107>.
 59. Hatakeyama, R., Péli-Gulli, M.P., Hu, Z., Jaquenoud, M., Garcia Osuna, G.M., Sardu, A., Dengjel, J., and De Virgilio, C. (2019). Spatially distinct pools of TORC1 balance protein homeostasis. *Mol. Cell* 73, 325–338. e8. <https://doi.org/10.1016/j.molcel.2018.10.040>.
 60. Cecil, J.H., Padilla, C.M., Lipinski, A.A., Langlais, P.R., Luo, X., and Capaldi, A.P. (2023). The molecular logic of Gtr1/2 and Pib2 dependent TORC1 regulation in budding yeast. Preprint at bioRxiv. <https://doi.org/10.1101/2023.12.06.570342>.
 61. Hughes Hallett, J.E., Luo, X., and Capaldi, A.P. (2014). State transitions in the TORC1 signaling pathway and information processing in *Saccharomyces cerevisiae*. *Genetics* 198, 773–786. <https://doi.org/10.1534/genetics.114.168369>.
 62. Kira, S., Tabata, K., Shirahama-Noda, K., Nozoe, A., Yoshimori, T., and Noda, T. (2014). Reciprocal conversion of Gtr1 and Gtr2 nucleotide-binding states by Npr2-Npr3 inactivates TORC1 and induces autophagy. *Autophagy* 10, 1565–1578. <https://doi.org/10.4161/auto.29397>.
 63. Sekiguchi, T., Kamada, Y., Furuno, N., Funakoshi, M., and Kobayashi, H. (2014). Amino acid residues required for Gtr1p-Gtr2p complex formation and its interactions with the Ego1p-Ego3p complex and TORC1 components in yeast. *Genes Cells* 19, 449–463. <https://doi.org/10.1111/gtc.12145>.
 64. Hatakeyama, R. (2021). Pib2 as an emerging master regulator of yeast TORC1. *Biomolecules* 11, 1489. <https://doi.org/10.3390/biom11101489>.
 65. Ukai, H., Araki, Y., Kira, S., Oikawa, Y., May, A.I., and Noda, T. (2018). Gtr/Ego-independent TORC1 activation is achieved through a glutamine-sensitive interaction with Pib2 on the vacuolar membrane. *PLoS Genet.* 14, e1007334. <https://doi.org/10.1371/journal.pgen.1007334>.
 66. Zeng, Q., Araki, Y., and Noda, T. (2024). Pib2 is a cysteine sensor involved in TORC1 activation in *Saccharomyces cerevisiae*. *Cell Rep.* 43, 113599. <https://doi.org/10.1016/j.celrep.2023.113599>.
 67. Tanigawa, M., and Maeda, T. (2017). An *in vitro* TORC1 kinase assay that recapitulates the Gtr-independent glutamine-responsive TORC1 activation mechanism on yeast vacuoles. *Mol. Cell Biol.* 37, e00075-17. <https://doi.org/10.1128/MCB.00075-17>.
 68. Tanigawa, M., Yamamoto, K., Nagatoishi, S., Nagata, K., Noshiro, D., Noda, N.N., Tsumoto, K., and Maeda, T. (2021). A glutamine sensor that directly activates TORC1. *Commun. Biol.* 4, 1093. <https://doi.org/10.1038/s42003-021-02625-w>.
 69. Troutman, K.K., Varlakhanova, N.V., Tornabene, B.A., Ramachandran, R., and Ford, M.G.J. (2022). Conserved Pib2 regions have distinct roles in TORC1 regulation at the vacuole. *J. Cell Sci.* 135, jcs259994. <https://doi.org/10.1242/jcs.259994>.
 70. Kim, A., and Cunningham, K.W. (2015). A LAPF/phafin1-like protein regulates TORC1 and lysosomal membrane permeabilization in response to endoplasmic reticulum membrane stress. *Mol. Biol. Cell* 26, 4631–4645. <https://doi.org/10.1091/mbc.E15-08-0581>.
 71. Michel, A.H., Hatakeyama, R., Kimmig, P., Arter, M., Peter, M., Matos, J., De Virgilio, C., and Kornmann, B. (2017). Functional mapping of yeast genomes by saturated transposition. *Elife* 6, e23570. <https://doi.org/10.7554/elife.23570>.
 72. Varlakhanova, N.V., Mihalevic, M.J., Bernstein, K.A., and Ford, M.G.J. (2017). Pib2 and the EGO complex are both required for activation of TORC1. *J. Cell Sci.* 130, 3878–3890. <https://doi.org/10.1242/jcs.207910>.
 73. Tarassov, K., Messier, V., Landry, C.R., Radinovic, S., Serna Molina, M., Shames, I., Malitskaya, Y., Vogel, J., Bussey, H., and Michnick, S.W. (2008). An *in vivo* map of the yeast protein interactome. *Science* 320, 1465–1470. <https://doi.org/10.1126/science.1153878>.
 74. Jumper, J., Evans, R., Pritzel, A., Green, T., Figurnov, M., Ronneberger, O., Tunyasuvunakool, K., Bates, R., Žídek, A., Potapenko, A., et al. (2021). Highly accurate protein structure prediction with AlphaFold. *Nature* 596, 583–589. <https://doi.org/10.1038/s41586-021-03819-2>.
 75. Varadi, M., Bertoni, D., Magana, P., Paramval, U., Pidruchna, I., Radhakrishnan, M., Tselenkov, M., Nair, S., Mirdita, M., Yeo, J., et al. (2024). AlphaFold protein structure database in 2024: providing structure coverage for over 214 million protein sequences. *Nucleic Acids Res.* 52, D368–D375. <https://doi.org/10.1093/nar/gkad1011>.
 76. Kira, S., Kumano, Y., Ukai, H., Takeda, E., Matsuura, A., and Noda, T. (2016). Dynamic relocation of the TORC1-Gtr1/2-Ego1/2/3 complex is regulated by Gtr1 and Gtr2. *Mol. Biol. Cell* 27, 382–396. <https://doi.org/10.1091/mbc.E15-07-0470>.
 77. Dokládal, L., Stumpe, M., Hu, Z., Jaquenoud, M., Dengjel, J., and De Virgilio, C. (2021). Phosphoproteomic responses of TORC1 target kinases reveal discrete and convergent mechanisms that orchestrate the quiescence program in yeast. *Cell Rep.* 37, 110149. <https://doi.org/10.1016/j.celrep.2021.110149>.
 78. Gerasimaite, R., and Mayer, A. (2016). Enzymes of yeast polyphosphate metabolism: structure, enzymology and biological roles. *Biochem. Soc. Trans.* 44, 234–239. <https://doi.org/10.1042/BST20150213>.
 79. Russnak, R., Konczal, D., and McIntire, S.L. (2001). A family of yeast proteins mediating bidirectional vacuolar amino acid transport. *J. Biol. Chem.* 276, 23849–23857. <https://doi.org/10.1074/jbc.M008028200>.
 80. Yang, M., Jensen, L.T., Gardner, A.J., and Culotta, V.C. (2005). Manganese toxicity and *Saccharomyces cerevisiae* Mam3p, a member of the ACDP (ancient conserved domain protein) family. *Biochem. J.* 386, 479–487. <https://doi.org/10.1042/BJ20041582>.

81. Petrezselyova, S., Kinclova-Zimmermannova, O., and Sychrova, H. (2013). Vhc1, a novel transporter belonging to the family of electroneutral cation-Cl⁻ cotransporters, participates in the regulation of cation content and morphology of *Saccharomyces cerevisiae* vacuoles. *Biochim. Biophys. Acta* 1828, 623–631. <https://doi.org/10.1016/j.bbamem.2012.09.019>.
82. Li, P., Wang, K., Salustros, N., Grönberg, C., and Gourdon, P. (2021). Structure and transport mechanism of P5B-ATPases. *Nat. Commun.* 12, 3973. <https://doi.org/10.1038/s41467-021-24148-y>.
83. Hedbacher, K., and Carlson, M. (2008). SNF1/AMPK pathways in yeast. *Front. Biosci.* 13, 2408–2420. <https://doi.org/10.2741/2854>.
84. Brito, A.S., Soto Diaz, S., Van Vooren, P., Godard, P., Marini, A.M., and Boeckstaens, M. (2019). Pib2-dependent feedback control of the TORC1 signaling network by the Npr1 kinase. *iScience* 20, 415–433. <https://doi.org/10.1016/j.isci.2019.09.025>.
85. MacGurn, J.A., Hsu, P.C., Smolka, M.B., and Emr, S.D. (2011). TORC1 regulates endocytosis via Npr1-mediated phosphoinhibition of a ubiquitin ligase adaptor. *Cell* 147, 1104–1117. <https://doi.org/10.1016/j.cell.2011.09.054>.
86. Hatakeyama, R., and De Virgilio, C. (2016). Unsolved mysteries of Rag GTPase signaling in yeast. *Small GTPases* 7, 239–246. <https://doi.org/10.1080/21541248.2016.1211070>.
87. Chen, Z., Malia, P.C., Hatakeyama, R., Nicastro, R., Hu, Z., Péli-Gulli, M. P., Gao, J., Nishimura, T., Eskes, E., Stefan, C.J., et al. (2021). TORC1 determines Fab1 lipid kinase function at signaling endosomes and vacuoles. *Curr. Biol.* 31, 297–309.e8. <https://doi.org/10.1016/j.cub.2020.10.026>.
88. Novarina, D., Guerra, P., and Milias-Argeitis, A. (2021). Vacuolar localization via the N-terminal domain of Sch9 is required for TORC1-dependent phosphorylation and downstream signal transduction. *J. Mol. Biol.* 433, 167326. <https://doi.org/10.1016/j.jmb.2021.167326>.
89. Jin, N., Mao, K., Jin, Y., Tevzadze, G., Kauffman, E.J., Park, S., Bridges, D., Loewith, R., Saltiel, A.R., Kionsky, D.J., and Weisman, L.S. (2014). Roles for PI(3,5)P₂ in nutrient sensing through TORC1. *Mol. Biol. Cell* 25, 1171–1185. <https://doi.org/10.1091/mbc.E14-01-0021>.
90. Napolitano, G., Di Malta, C., and Ballabio, A. (2022). Non-canonical mTORC1 signaling at the lysosome. *Trends Cell Biol.* 32, 920–931. <https://doi.org/10.1016/j.tcb.2022.1004.1012>.
91. Acharya, A., and Demetriades, C. (2024). mTORC1 activity licenses its own release from the lysosomal surface. *Mol. Cell* 84, 4385–4400.e7. <https://doi.org/10.1016/j.molcel.2024.10.008>.
92. Zwakenberg, S., Westland, D., van Es, R.M., Rehmann, H., Anink, J., Cia-paite, J., Bosma, M., Stelloo, E., Liv, N., Sobrevals Alcaraz, P., et al. (2024). mTORC1 restricts TFE3 activity by auto-regulating its presence on lysosomes. *Mol. Cell* 84, 4368–4384.e6. <https://doi.org/10.1016/j.molcel.2024.10.009>.
93. Fernandes, S.A., Angelidaki, D.D., Nüchel, J., Pan, J., Gollwitzer, P., Elkis, Y., Artoni, F., Wilhelm, S., Kovacevic-Sarmiento, M., and Demetriades, C. (2024). Spatial and functional separation of mTORC1 signaling in response to different amino acid sources. *Nat. Cell Biol.* 26, 1918–1933. <https://doi.org/10.1038/s41556-024-01523-7>.
94. Bridges, D., Ma, J.T., Park, S., Inoki, K., Weisman, L.S., and Saltiel, A.R. (2012). Phosphatidylinositol 3,5-bisphosphate plays a role in the activation and subcellular localization of mechanistic target of rapamycin 1. *Mol. Biol. Cell* 23, 2955–2962. <https://doi.org/10.1091/mbc.E11-12-1034>.
95. Liang, R., Ren, J., Zhang, Y., and Feng, W. (2019). Structural conservation of the two phosphoinositide-binding sites in WIPI proteins. *J. Mol. Biol.* 431, 1494–1505. <https://doi.org/10.1016/j.jmb.2019.02.019>.
96. Prouteau, M., Bourgoïnt, C., Félix, J., Bonadei, L., Sadian, Y., Gabus, C., Savvides, S.N., Gutsche, I., Desfosses, A., and Loewith, R. (2023). EGOC inhibits TOROID polymerization by structurally activating TORC1. *Nat. Struct. Mol. Biol.* 30, 273–285. <https://doi.org/10.1038/s41594-022-00912-6>.
97. Prouteau, M., Desfosses, A., Sieben, C., Bourgoïnt, C., Lydia Mozaffari, N., Demurtas, D., Mitra, A.K., Guichard, P., Manley, S., and Loewith, R. (2017). TORC1 organized in inhibited domains (TOROIDs) regulate TORC1 activity. *Nature* 550, 265–269. <https://doi.org/10.1038/nature24021>.
98. Sullivan, A., Wallace, R.L., Wellington, R., Luo, X., and Capaldi, A.P. (2019). Multilayered regulation of TORC1-body formation in budding yeast. *Mol. Biol. Cell* 30, 400–410. <https://doi.org/10.1091/mbc.E18-05-0297>.
99. Zhang, T., Péli-Gulli, M.P., Yang, H., De Virgilio, C., and Ding, J. (2012). Ego3 functions as a homodimer to mediate the interaction between Gtr1-Gtr2 and Ego1 in the EGO complex to activate TORC1. *Structure* 20, 2151–2160. <https://doi.org/10.1016/j.str.2012.09.019>.
100. Yerlikaya, S., Meusburger, M., Kumari, R., Huber, A., Anrather, D., Costanzo, M., Boone, C., Ammerer, G., Baranov, P.V., and Loewith, R. (2016). TORC1 and TORC2 work together to regulate ribosomal protein S6 phosphorylation in *Saccharomyces cerevisiae*. *Mol. Biol. Cell* 27, 397–409. <https://doi.org/10.1091/mbc.E15-08-0594>.
101. Brachmann, C.B., Davies, A., Cost, G.J., Caputo, E., Li, J., Hieter, P., and Boeke, J.D. (1998). Designer deletion strains derived from *Saccharomyces cerevisiae* S288C: a useful set of strains and plasmids for PCR-mediated gene disruption and other applications. *Yeast* 14, 115–132. [https://doi.org/10.1002/\(SICI\)1097-0061\(19980130\)14:2<115::AID-YEA204>3.0.CO;2-2](https://doi.org/10.1002/(SICI)1097-0061(19980130)14:2<115::AID-YEA204>3.0.CO;2-2).
102. Hatakeyama, R., and De Virgilio, C. (2019). TORC1 specifically inhibits microautophagy through ESCRT-0. *Curr. Genet.* 65, 1243–1249. <https://doi.org/10.1007/s00294-019-00982-y>.
103. Wach, A., Brachat, A., Pöhlmann, R., and Philippse, P. (1994). New heterologous modules for classical or PCR-based gene disruptions in *Saccharomyces cerevisiae*. *Yeast* 10, 1793–1808. <https://doi.org/10.1002/yea.320101310>.
104. Wach, A., Brachat, A., Alberti-Segui, C., Reibischung, C., and Philippse, P. (1997). Heterologous HIS3 marker and GFP reporter modules for PCR-targeting in *Saccharomyces cerevisiae*. *Yeast* 13, 1065–1075. [https://doi.org/10.1002/\(SICI\)1097-0061\(19970915\)13:11<1065::AID-YEA159>3.0.CO;2-K](https://doi.org/10.1002/(SICI)1097-0061(19970915)13:11<1065::AID-YEA159>3.0.CO;2-K).
105. Longtine, M.S., McKenzie, A., 3rd, Demarini, D.J., Shah, N.G., Wach, A., Brachat, A., Philippse, P., and Pringle, J.R. (1998). Additional modules for versatile and economical PCR-based gene deletion and modification in *Saccharomyces cerevisiae*. *Yeast* 14, 953–961. [https://doi.org/10.1002/\(SICI\)1097-0061\(199807\)14:10<953::AID-YEA293>3.0.CO;2-U](https://doi.org/10.1002/(SICI)1097-0061(199807)14:10<953::AID-YEA293>3.0.CO;2-U).
106. Wosika, V., Durandau, E., Varidel, C., Aymoz, D., Schmitt, M., and Pelet, S. (2016). New families of single integration vectors and gene tagging plasmids for genetic manipulations in budding yeast. *Mol. Genet. Genomics* 291, 2231–2240. <https://doi.org/10.1007/s00438-016-1249-1>.
107. Generoso, W.C., Gottardi, M., Oreb, M., and Boles, E. (2016). Simplified CRISPR-Cas genome editing for *Saccharomyces cerevisiae*. *J. Microbiol. Methods* 127, 203–205. <https://doi.org/10.1016/j.mimet.2016.06.020>.
108. Smets, B., Ghillebert, R., De Snijder, P., Bindu, M., Swinnen, E., De Virgilio, C., and Winderickx, J. (2010). Life in the midst of scarcity: adaptations to nutrient availability in *Saccharomyces cerevisiae*. *Curr. Genet.* 56, 1–32. <https://doi.org/10.1007/s00294-009-0287-1>.
109. Huang, J., and Mackerell, A.D., Jr. (2013). CHARMM36 all-atom additive protein force field: validation based on comparison to NMR data. *J. Comput. Chem.* 34, 2135–2145. <https://doi.org/10.1002/jcc.23354>.
110. Bindea, G., Mlecnik, B., Hackl, H., Charoentong, P., Tosolini, M., Kirillovsky, A., Friedman, W.H., Pagès, F., Trajanoski, Z., and Galon, J. (2009). ClueGO: a Cytoscape plug-in to decipher functionally grouped gene ontology and pathway annotation networks. *Bioinformatics* 25, 1091–1093. <https://doi.org/10.1093/bioinformatics/btp101>.

111. Shannon, P., Markiel, A., Ozier, O., Baliga, N.S., Wang, J.T., Ramage, D., Amin, N., Schwikowski, B., and Ideker, T. (2003). Cytoscape: a software environment for integrated models of biomolecular interaction networks. *Genome Res.* 13, 2498–2504. <https://doi.org/10.1101/gr.1239303>.
112. Cox, J., and Mann, M. (2008). MaxQuant enables high peptide identification rates, individualized p.p.b.-range mass accuracies and proteome-wide protein quantification. *Nat. Biotechnol.* 26, 1367–1372. <https://doi.org/10.1038/nbt.1511>.
113. Legeay, M., Doncheva, N.T., Morris, J.H., and Jensen, L.J. (2020). Visualize omics data on networks with Omics Visualizer, a Cytoscape App. *F1000Res.* 9, 157. <https://doi.org/10.12688/f1000research.22280.2>.
114. Janke, C., Magiera, M.M., Rathfelder, N., Taxis, C., Reber, S., Maekawa, H., Moreno-Borchart, A., Doenges, G., Schwob, E., Schiebel, E., and Knop, M. (2004). A versatile toolbox for PCR-based tagging of yeast genes: new fluorescent proteins, more markers and promoter substitution cassettes. *Yeast* 21, 947–962. <https://doi.org/10.1002/yea.1142>.
115. Evans, R., O'Neill, M., Pritzel, A., Antropova, N., Senior, A., Green, T., Žídek, A., Bates, R., Blackwell, S., Yim, J., et al. (2022). Protein complex prediction with AlphaFold-Multimer. Preprint at bioRxiv. <https://doi.org/10.1101/2021.10.04.463034>.
116. Mark, P., and Nilsson, L. (2002). Structure and dynamics of liquid water with different long-range interaction truncation and temperature control methods in molecular dynamics simulations. *J. Comput. Chem.* 23, 1211–1219. <https://doi.org/10.1002/jcc.10117>.
117. Bussi, G., Donadio, D., and Parrinello, M. (2007). Canonical sampling through velocity rescaling. *J. Chem. Phys.* 126, 014101. <https://doi.org/10.1063/1.2408420>.
118. Berendsen, H.J.C., Postma, J.P.M., Vangunsteren, W.F., Dinola, A., and Haak, J.R. (1984). Molecular-dynamics with coupling to an external bath. *J. Chem. Phys.* 81, 3684–3690. <https://doi.org/10.1063/1.448118>.
119. Parrinello, M., and Rahman, A. (1981). Polymorphic transitions in single-crystals - a new molecular-dynamics method. *J. Appl. Phys.* 52, 7182–7190. <https://doi.org/10.1063/1.328693>.
120. Darden, T., York, D., and Pedersen, L. (1993). Particle Mesh Ewald - an N. Log(N) Method for Ewald Sums in Large Systems. *J. Chem. Phys.* 98, 10089–10092. <https://doi.org/10.1063/1.464397>.
121. Brunn, G.J., Williams, J., Sabers, C., Wiederrecht, G., Lawrence, J.C., Jr., and Abraham, R.T. (1996). Direct inhibition of the signaling functions of the mammalian target of rapamycin by the phosphoinositide 3-kinase inhibitors, wortmannin and LY294002. *EMBO J.* 15, 5256–5267.
122. Wisniewski, J.R., Zougman, A., Nagaraj, N., and Mann, M. (2009). Universal sample preparation method for proteome analysis. *Nat. Methods* 6, 359–362. <https://doi.org/10.1038/nmeth.1322>.
123. Dokládal, L., Stumpe, M., Pillet, B., Hu, Z., Garcia Osuna, G.M., Kressler, D., Dengjel, J., and De Virgilio, C. (2021). Global phosphoproteomics pinpoints uncharted Gcn2-mediated mechanisms of translational control. *Mol. Cell* 81, 1879–1889.e6. <https://doi.org/10.1016/j.molcel.2021.02.037>.
124. Perez-Riverol, Y., Bandla, C., Kundu, D.J., Kamatchinathan, S., Bai, J., Hewapathirana, S., John, N.S., Prakash, A., Walzer, M., Wang, S., and Vizcaíno, J.A. (2025). The PRIDE database at 20 years: 2025 update. *Nucleic Acids Res.* 53, D543–D553. <https://doi.org/10.1093/nar/gkae1011>.
125. Perez-Riverol, Y., Csordas, A., Bai, J., Bernal-Llinares, M., Hewapathirana, S., Kundu, D.J., Inuganti, A., Griss, J., Mayer, G., Eisenacher, M., et al. (2019). The PRIDE database and related tools and resources in 2019: improving support for quantification data. *Nucleic Acids Res.* 47, D442–D450. <https://doi.org/10.1093/nar/gky1106>.
126. Bindea, G., Galon, J., and Mlecnik, B. (2013). CluePedia Cytoscape plugin: pathway insights using integrated experimental and in silico data. *Bioinformatics* 29, 661–663. <https://doi.org/10.1093/bioinformatics/btt019>.
127. Szklarczyk, D., Kirsch, R., Koutrouli, M., Nastou, K., Mehryary, F., Hachilif, R., Gable, A.L., Fang, T., Doncheva, N.T., Pyysalo, S., et al. (2023). The STRING database in 2023: protein-protein association networks and functional enrichment analyses for any sequenced genome of interest. *Nucleic Acids Res.* 51, D638–D646. <https://doi.org/10.1093/nar/gkac1000>.

STAR★METHODS

KEY RESOURCES TABLE

REAGENT or RESOURCE	SOURCE	IDENTIFIER
Antibodies		
Rabbit polyclonal anti-Sch9-pThr ⁷³⁷ (1:10'000)	De Virgilio lab	N/A
Goat polyclonal anti-Sch9 (1:1'000)	De Virgilio lab	N/A
Rabbit polyclonal anti-Adh1 (1:50'000)	Calbiochem	Cat# 126745-1ML; RRID:AB_11214375
Mouse monoclonal anti-HA (16B12) (1:1'000)	ENZO	Cat# ENZ-ABS120; RRID:AB_3076549
Mouse monoclonal anti-c-Myc (9E10) (1:3'000)	Santa Cruz Biotechnologies	Cat# sc-40; RRID:AB_627268
Mouse polyclonal anti-GFP (1:3'000)	Roche	Cat# 11814460001; RRID:AB_390913
Mouse monoclonal anti-tetra-His (1:1'000)	Qiagen	Cat# 34670; RRID:AB_2571551
Rabbit polyclonal anti-GST (1:3'000)	Bethyl	Cat# A190-122A; RRID:AB_67419
Rabbit polyclonal anti-Gtr1 (1:1'000)	De Virgilio lab	N/A
Rabbit polyclonal anti-Gtr2 (1:1'000)	De Virgilio lab	N/A
Rabbit polyclonal anti-ubiquitin (1:10'000)	Proteintech	Cat# 80992-1-RR; RRID:AB_2923694
Goat anti-mouse IgG-HRP conjugate (1:3'000)	Bio-Rad	Cat# 1706516; RRID:AB_2921252
Goat anti-rabbit IgG-HRP conjugate (1:3'000)	Bio-Rad	Cat# 1706515; RRID:AB_11125142
Rabbit anti-goat IgG-HRP conjugate (1:3'000)	Bio-Rad	Cat# 1721034; RRID:AB_2617114
Bacterial strains		
<i>E. coli</i> DH5α	CGSC	12384
<i>E. coli</i> Rosetta (DE3)	Novagen	70954
Chemicals, peptides, and recombinant proteins		
AgaPure Agarose LE	Canvax	AG006
Agar	Formedium	AGA03
Ammonium sulfate	MP Biomedicals	4808211
Arg6	Sigma-Aldrich	643440
Arg10	Sigma-Aldrich	608033
Bromophenol Blue	Fluka	810336
C18 Cartridges	Macherey-Nagel	731802
ChamQ Universal SYBR qPCR Master Mixsupermix	Vazyme	Q711-03
Complete EDTA-free Protease Inhibitor Cocktail	Roche	11-697-498-001
Cycloheximide	Sigma-Aldrich	C7698-5G
D(+)-Glucose anhydrous	AppliChem	A1422
Drop-out Mix Synthetic, minus Ade, His, Leu, Trp, Ura w/o YNB	US Biological	D9540-05
Drop-out Mix Synthetic, minus His w/o YNB	US Biological	D9520
DTT	AppliChem	A1101
FM4-64	Invitrogen	T-3166
GFP-trap Agarose Beads	ChromoTek	gta-20
Glutathione MagBeads	GenScript	L00327
Glycerol	Sigma-Aldrich	49770
Glycine	AppliChem	A1067
HR-X Column	Macherey-Nagel	730936P45
LB Broth (Lennox)	CONDA	1231
Lys4	Sigma-Aldrich	616192
Lys8	Sigma-Aldrich	608041

(Continued on next page)

Continued

REAGENT or RESOURCE	SOURCE	IDENTIFIER
Lys-C	FUJIFILM Wako	129-02541
MG-132	Sigma-Aldrich	474787
Nonidet P-40	AppliChem	A1694
Pefabloc	Sigma-Aldrich	76307
PEG	Sigma-Aldrich	81240
Phire polymerase	Thermo Scientific	F1124
PhosSTOP	Roche	04-906-837-001
Phusion polymerase	Thermo Scientific	F5302
Pierce Anti-HA Magnetic Beads	Thermo Scientific	88837
Rabbit IgGs	Sigma-Aldrich	I5006
Rapamycin	LC Laboratories	R-5000
RedSafe Nucleic Acid Staining	iNtRON	21141
ReproSil-Pur 120 C18-AQ, 1.9 mm	Dr. Maisch	r119.aq
SDS	Sigma-Aldrich	75746
SYPRO Ruby Protein Gel Stain	Sigma-Aldrich	S4942
TCA	Sigma-Aldrich	27242
TiO ₂	GL Sciences	5020-75010
Trizma base	Sigma-Aldrich	T1503
Trypsin	Promega	V5113
Tween 20	AppliChem	A4974
Urea	Sigma-Aldrich	33247
Yeast nitrogen base	CONDA	1545
YPD Broth	US Biological	Y2075
Critical commercial assays		
Lambda Protein Phosphatase kit	New England Biolabs	P0753S
ECL Western Blotting Detection	GE Healthcare	RPN2106
Radiance Plus Sensitive ECL	Azure Biosystems	AC2103
iScript cDNA Synthesis Kit	Bio-Rad	1708890
Deposited data		
Raw Data	Mendeley Data Link	https://doi.org/10.17632/nbc2yff7w8.1
MS-RAW files	ProteomeXchange	PXD059088
Experimental models: Organisms/strains		
BY4741	Euroscarf	[BY4741] MAT α ; his3Δ1, leu2Δ0, met15Δ0, ura3Δ0
YL515	Binda et al. ¹⁶	MAT α ; his3Δ1, leu2Δ0, ura3Δ0
YL516	Binda et al. ¹⁶	MAT α ; his3Δ1, leu2Δ0, ura3Δ0
NIC104	This study	[YL516] TCO89-HA ₃ ::HIS3
NIC119	This study	[YL515] TCO89-HA ₃ ::HIS3
NIC230	This study	[NIC119] ssh4Δ::kanMX
MJA741	This study	[NIC119] atg1Δ::kanMX
MJA742	This study	[NIC119] atg19Δ::kanMX
tor1Δ-6C	C. De Virgilio lab	[YL515] tor1Δ::kanMX
NIC169	This study	[tor1Δ-6C] LEU2::TOR1p-HA ₃ -TOR1
NIC087	This study	[YL515] KOG1-HA ₃ ::HIS3
MPG56	Binda et al. ¹⁶	[YL516] TCO89-GFP::kanMX
MPG8453	This study	[MPG56] [HIS3::VAC8p-yEmRFP-TOR1]
MPG8452	This study	[MPG8453] gtr1Δ::kanMX, gtr2Δ::KanMX
NIC235	This study	[YL516] TCO89-myc ₁₃ ::HIS3

(Continued on next page)

Continued

REAGENT or RESOURCE	SOURCE	IDENTIFIER
NIC210	This study	[NIC119] <i>pdr5Δ::kanMX</i>
MC477	This study	[NIC210] <i>erg6Δ::hphNT1</i>
MP06-8B	Binda et al. ¹⁶	[YL516] <i>gtr1Δ::kanMX6, gtr2Δ::kanMX6</i>
MC466	This study	[MP06-8B] <i>tco89Δ::hphNT1</i>
MC478	This study	[MC466] <i>LEU2::TOR1p-GFP-TOR1</i>
MC479	This study	[MC478] <i>URA3::TCO89p-TCO89-HA₃</i>
NIC076	This study	[YL515] <i>tco89Δ::hphNT1</i>
NIC167	This study	[NIC119] <i>tco89^{K276R,K279R}-HA₃::HIS3</i>
NIC134	This study	[NIC076] <i>LEU2</i>
NIC135	This study	[NIC076] <i>LEU2::TCO89p-TCO89</i>
NIC136	This study	[NIC076] <i>LEU2::TCO89p-tco89^{23A}</i>
NIC164	This study	[NIC076] <i>LEU2::TCO89p-tco89^{23E}</i>
NIC140	This study	[NIC135] <i>TCO89:HA₃::HIS3</i>
NIC141	This study	[NIC136] <i>tco89^{23A}-HA₃::HIS3</i>
NIC166	This study	[NIC164] <i>tco89^{23E}-HA₃::HIS3</i>
RKH315	C. De Virgilio lab	[BY4741] <i>tco89Δ::kanMX, LEU2::TOR1p-GFP-TOR1</i>
NIC183	This study	[RKH315] <i>URA3::TCO89p-TCO89</i>
NIC184	This study	[RKH315] <i>URA3::TCO89p-tco89^{23A}</i>
NIC185	This study	[RKH315] <i>URA3::TCO89p-tco89^{23E}</i>
NIC186	This study	[NIC183] <i>TCO89-HA₃::HIS3</i>
NIC190	This study	[NIC184] <i>tco89^{23A}-HA₃::HIS3</i>
NIC187	This study	[NIC185] <i>tco89^{23E}-HA₃::HIS3</i>
NIC198	This study	[NIC135] <i>TCO89-GFP::HIS3</i>
NIC207	This study	[NIC198] <i>VPH1-mCherry::URA3</i>
NIC199	This study	[NIC136] <i>tco89^{23A}-GFP::HIS3</i>
NIC200	This study	[NIC164] <i>tco89^{23E}-GFP::HIS3</i>
NIC193	This study	[NIC183] <i>VPH1-mCherry::HIS3</i>
NIC142	This study	[NIC119] <i>gtr1Δ::HIS3, gtr2Δ::hphNT1</i>
NIC022	This study	[YL516] <i>gtr1^{S20L}</i>
NIC259	This study	[NIC022] <i>tco89Δ::hphNT1</i>
NIC159	This study	[NIC140] <i>gtr1Δ::kanMX, gtr2Δ::URA3</i>
NIC160	This study	[NIC141] <i>gtr1Δ::kanMX, gtr2Δ::URA3</i>
NIC216	This study	[NIC166] <i>gtr1Δ::kanMX, gtr2Δ::URA3</i>
NIC221	This study	[NIC119] <i>pib2Δ::URA3</i>
NIC223	This study	[NIC076] <i>LEU2::TCO89p-tco89⁵⁸⁵⁻⁷⁹⁹</i>
NIC224	This study	[NIC223] <i>tco89⁵⁸⁵⁻⁷⁹⁹-HA₃::HIS3</i>
NIC238	This study	[NIC223] <i>tco89⁵⁸⁵⁻⁷⁹⁹-GFP::HIS3</i>
NIC241	This study	[RKH315] <i>URA3::TCO89p-tco89⁵⁸⁵⁻⁷⁹⁹</i>
NMY51	Dualsystems Biotech AG	<i>MATA; his3Δ200 trp1-901, leu2-3, 112, ade2, LYS::(lexAop)4-HIS3, ura3::(lexAop)8-lacZ, ade2::(lexAop)8-ADE2, GAL4</i>
RKH96	This study	[NMY51] <i>gtr1Δ::kanMX</i>
RKH98	This study	[NMY51] <i>gtr2Δ::kanMX</i>
RKH100	This study	[NMY51] <i>ego1Δ::kanMX</i>
RKH102	This study	[NMY51] <i>ego2Δ::kanMX</i>
MPG2952	Zhang et al. ⁹⁹	[NMY51] <i>ego3Δ::kanMX</i>
NIC222	This study	[NIC119] <i>tco89^{S589A,R590A,T591A,Q592A,K594A}</i>
NIC225	This study	[NIC142] <i>tco89^{S589A,R590A,T591A,Q592A,K594A}</i>
NIC236	This study	[YL516] <i>tco89^{S589A,R590A,T591A,Q592A,K594A}</i>
NIC243	This study	[NIC236] <i>tco89^{S589A,R590A,T591A,Q592A,K594A}-GFP::HIS3</i>

(Continued on next page)

Continued

REAGENT or RESOURCE	SOURCE	IDENTIFIER
NIC250	This study	[NIC243] <i>VPH1::mCherry::URA3</i>
RKH395	Hatakeyama et al. ⁵⁹	[YL516] <i>LEU2::TOR1p-GFP-TOR1</i>
MC225	C. De Virgilio Lab	[RKH225] <i>VPH1-mCherry::URA3</i>
NIC294	This study	[NIC236] <i>LEU2::TOR1p-GFP-TOR1</i>
NIC261	This study	[YL516] <i>tco89^{E647A,R651A,E721A,N726A,D728A}</i>
NIC274	This study	[NIC119] <i>tco89^{E647A,R651A,E721A,N726A,D728A}</i>
NIC283	This study	[NIC261] <i>tco89^{E647A,R651A,E721A,N726A,D728A}-GFP::HIS3</i>
MC227	C. De Virgilio Lab	[MP56] <i>VPH1-mCherry::URA3</i>
NIC296	This study	[NIC261] <i>LEU2::TOR1p-GFP-TOR1</i>
NIC228	This study	[NIC119] <i>tco89^{E647A,R651A}</i>
NIC331	This study	[NIC076] <i>LEU2::TCO89p-tco89^{S589A,R590A,T591A,Q592A,K594A}</i>
NIC338	This study	[NIC331] <i>tco89^{S589A,R590A,T591A,Q592A,K594A}-HA₃::HIS3</i>
NIC277	This study	[NIC141] <i>tco89^{23A,S589A,R590A,T591A,Q592A,K594A}</i>
NIC271	This study	[NIC166] <i>tco89^{23E,S589A,R590A,T591A,Q592A,K594A}</i>
NIC237	This study	[YL516] <i>tco89^{E647A,R651A}</i>
NIC244	This study	[NIC237] <i>tco89^{E647A,R651A}-GFP::HIS3</i>
NIC251	This study	[NIC244] <i>VPH1-mCherry::URA3</i>
NIC237	This study	[YL516] <i>tco89^{E647A,R651A}</i>
NIC295	This study	[NIC237] <i>LEU2::TOR1p-GFP-TOR1</i>
NIC267	This study	[NIC140] <i>tco89^{E647A,R651A,E721A,N726A,D728A}</i>
NIC291	This study	[NIC136] <i>tco89^{23A, E647A,R651A,E721A,N726A,D728A}</i>
NIC339	This study	[NIC164] <i>tco89^{23E, E647A,R651A,E721A,N726A,D728A}</i>
NIC302	This study	[NIC291] <i>tco89^{23A, E647A,R651A,E721A,N726A,D728A}-HA₃::HIS3</i>
NIC340	This study	[NIC339] <i>tco89^{23E, E647A,R651A,E721A,N726A,D728A}-HA₃::HIS3</i>
RKH323	Hatakeyama et al. ⁵⁹	[YL516] <i>PIB2-200-yEmRFP</i>
RKH362	Hatakeyama et al. ⁵⁹	[RKH323] <i>LEU2::TOR1p-GFP-TOR1</i>
SF7988	This study	[RKH362] <i>tco89Δ::hphNT1</i>
NIC327	This study	[RKH323] <i>tco89Δ::hphNT1</i>
NIC305	This study	[NIC183] <i>pib2Δ::kanMX</i>
NIC307	This study	[NIC185] <i>pib2Δ::kanMX</i>
yRL393	This study	[YL516] <i>tco89Δ::kanMX, GFP-GTR1</i>
yRL400	This study	<i>tco89Δ::kanMX, PIB2-200-EGFP</i>
RL170-2C	Yerlikaya et al. ¹⁰⁰	[TB50] <i>TCO89-TAP::TRP1, leu2-3, ura3-52, trp1, his3, rme1</i>
MJ5682	Hu et al. ⁴⁴	[YL516] <i>arg4Δ::HIS3, lys2Δ::hphNT1</i>
S288C	Brachmann et al. ¹⁰¹	<i>MATα; SUC2, gal2, mal2, mel, flo1, flo8-1, hap1, ho, bio1, bio6</i>
MC468	This study	[SC288C] <i>rpn5^{ts}, HIS3::TCO89p-TCO89-HA₃</i>
MJA758	This study	[SC288C] <i>pup1^{ts}, HIS3::TCO89p-TCO89-HA₃</i>
MJA743	This study	[NIC076] <i>URA3::TCO89p-TCO89-HA₃</i>
MC472	This study	[NIC076] <i>URA3::TCO89p-tco89^{K58R}-HA₃</i>
MP06-8B	Binda et al. ¹⁶	[YL516] <i>gtr2Δ::kanMX6, gtr2Δ::kanMX6</i>
MC466	This study	[MP06-8B] <i>tco89Δ::hphNT1</i>
MJA752	This study	[MC466] <i>URA3::TCO89p-TCO89-HA₃</i>
MC478	This study	[MC466] <i>LEU2::TOR1p-GFP-TOR1</i>
MC479	This study	[MC478] <i>URA3::TCO89p-TCO89-HA₃</i>
LD6663	This study	[MJ5682] <i>tco89Δ::kanMX</i>

Oligonucleotides

See Table S5 for the list of oligonucleotides

(Continued on next page)

Continued

REAGENT or RESOURCE	SOURCE	IDENTIFIER
Recombinant DNA		
pRS413	Brachmann et al. ¹⁰¹	CEN/ARS, <i>HIS3</i>
pRS415	Brachmann et al. ¹⁰¹	CEN/ARS, <i>LEU2</i>
pRS416	Brachmann et al. ¹⁰¹	CEN/ARS, <i>URA3</i>
pRS413-MET15	Hatakeyama et al. ¹⁰²	[pRS413] <i>MET15</i>
pFA6a-kanMX6	Wach et al. ¹⁰³	<i>TEFp-kanMX6-TEFt</i>
pFA6a-HIS3	Wach et al. ¹⁰⁴	<i>TEFp-HIS3MX6-TEFt</i>
pFA6a-hphNT1	C. De Virgilio Lab	<i>TEFp-hphNT1-TEFt</i>
pFA6a-URA3	C. De Virgilio Lab	<i>TEFp-URA3-TEFt</i>
pFA6a-GFP-kanMX	Longtine et al. ¹⁰⁵	<i>GFP-ADH1t-TEFp-kanMX6-TEFt</i>
pFA6a-GFP-HIS3	Longtine et al. ¹⁰⁵	<i>GFP-ADH1t-TEFp-HIS3MX6-TEFt</i>
pFA6a-myc ₁₃ -HIS	Longtine et al. ¹⁰⁵	<i>myc₁₃-ADH1t-TEFp-HIS3MX6-TEFt</i>
pFA6a-HA ₃ -HIS3	Longtine et al. ¹⁰⁵	<i>HA₃-ADH1t-TEFp-HIS3MX6-TEFt</i>
pGTU-r	Wosika et al. ¹⁰⁶	<i>mCherry-ADH1t-TEFp-URA3-TEFt</i>
pGTH-r	Wosika et al. ¹⁰⁶	<i>mCherry-ADH1t-TEFp-HIS3-TEFt</i>
pSIVI	Wosika et al. ¹⁰⁶	<i>LEU2p-TEFp-LEU2-TEFt-MCS-LEU2t</i>
pSIVu	Wosika et al. ¹⁰⁶	<i>URA3p-TEFp-URA3-TEFt-MCS-URA3t</i>
pSIVh	Wosika et al. ¹⁰⁶	<i>HIS3 shortp-TEFp-SpHIS5-TEFt-MCS1-HIS3t</i>
pSF4847	This study	[pSIVh] <i>VAC8p-yEmRFP-TOR1</i>
pNIC040	This study	[pSIVI] <i>TOR1p-HA₃-TOR1-TOR1t</i>
pNIC021	This study	[pSIVI] <i>TCO89p-TCO89-TCO89t</i>
pNIC022	This study	[pSIVI] <i>TCO89p-tco89^{23A}-TCO89t</i>
pNIC035	This study	[pSIVI] <i>TCO89p-tco89^{23E}-TCO89t</i>
pNIC050	This study	[pSIVI] <i>TCO89p-tco89⁵⁸⁵⁻⁷⁹⁹-TCO89t</i>
pNIC075	This study	[pSIVI] <i>TCO89p-tco89^{S589A,R590A,T591A,Q592A,K594A}-TCO89t</i>
pNIC076	This study	[pSIVI] <i>TCO89p-tco89^{E647A,R651A,E721A,N726A,D728A}-TCO89t</i>
pNIC068	This study	[pSIVI] <i>TCO89p-tco89^{23A,E647A,R651A,E721A,N726A,D728A}-TCO89t</i>
pNIC069	This study	[pSIVI] <i>TCO89p-tco89^{23E,E647A,R651A,E721A,N726A,D728A}-TCO89t</i>
pNIC042	This study	[pSIVu] <i>TCO89p-TCO89-TCO89t</i>
pNIC043	This study	[pSIVu] <i>TCO89p-tco89^{23A}-TCO89t</i>
pNIC044	This study	[pSIVu] <i>TCO89p-tco89^{23E}-TCO89t</i>
pNIC055	This study	[pSIVu] <i>TCO89p-tco89⁵⁸⁵⁻⁷⁹⁹-TCO89t</i>
pRCC-K	AddGene, Generoso et al. ¹⁰⁷	<i>2μ, kanMX, ROX3p-CAS9-CYC1t, SNR52-gRNA</i>
pNIC002	This study	[pRCC-K] <i>gtr1^{S20L}-gRNA</i>
pNIC039	This study	[pRCC-K] <i>tco89^{K276,K279}-gRNA</i>
pNIC049	This study	[pRCC-K] <i>tco89^{S589,R590,T591,Q592,K594}-gRNA</i>
pNIC055	This study	[pRCC-K] <i>tco89^{E647,R651}-gRNA</i>
pNIC064	This study	[pRCC-K] <i>tco89^{E721,N726,D728}-gRNA</i>
pSK108	Kira et al. ⁶²	<i>LEU2-TOR1p-GFP-TOR1¹⁻⁴²⁶</i>
pCabWT	Dualsystems Biotech AG	<i>CEN/ARS, LEU2, Aβ-Cub-LexA-VP16</i>
pPR3-N	Dualsystems Biotech AG	<i>2 μ, TRP1, NubG-HA</i>
pDL2-ALG5	Dualsystems Biotech AG	<i>2 μ, TRP1, ALG5-NubG-HA</i>
pAI-ALG5	Dualsystems Biotech AG	<i>2 μ, TRP1, ALG5-NubI-HA</i>
pPR3-N-GTR1-WT	Binda et al. ¹⁶	[pPR3-N] <i>GTR1</i>
pPR3-N-GTR2-WT	Binda et al. ¹⁶	[pPR3-N] <i>GTR2</i>

(Continued on next page)

Continued

REAGENT or RESOURCE	SOURCE	IDENTIFIER
pPR3-KOG1	Michel et al. ⁷¹	[pPR3-N] KOG1
pCabWT-TCO89	Binda et al. ¹⁶	[pCabWT] TCO89
pNIC060	This study	[pCabWT] tco89 ^{S589A,R590A,T591A,Q592A,K594A}
pNIC058	This study	[pCabWT] tco89 ^{S589A,R590A,T591A,Q592A,K594A}
pNIC059	This study	[pCabWT] tco89 ^{E647A,R654A}
pNIC066	This study	[pCabWT] tco89 ^{E647A,R651A,E721A,N726A,D728A}
pCAB-PIB2	Michel et al. ⁷¹	[pCabWT] PIB2
pPR3-N-EGO1	This study	[pPR3-N] EGO1
pPR3-N-EGO2	This study	[pPR3-N] EGO2
pMPG2221	Zhang et al. ⁹⁹	[pPR3-N] EGO3
pPR3-N-GTR1-1-184	This study	[pPR3-N] GTR1 ¹⁻¹⁸⁴
pPR3-N-GTR1-180-311	This study	[pPR3-N] GTR1 ¹⁸⁰⁻³¹¹
pNP1690	Binda et al. ¹⁶	[pPR3-N] GTR1 ^{S20L}
pNP1691	Binda et al. ¹⁰⁸	[pPR3-N] GTR1 ^{Q65L}
pET41a(+) - TCO89-585-799	This study	[pET41+] GST-TCO89 ^{S585-799}
pET41a(+) - TCO89-585-799_5A	This study	[pET41+] GST-tco ^{S585-799,S589A,R590A,T591A,Q592A,K594A}
pETDuet-1-GTR1-GTR2	C. De Virgilio Lab	[pETDuet-1] GTR1 GTR2
pNIC070	This study	[pETDuet-1] His ₆ -KOG1 ^{I536-T082}
pSF4871	This study	pSIVu-SCH9p-mNeonGreen-(GA)5-SCH9-ADH1ter
pMJA4946	This study	[pSIVu] TCO89p-TCO89-HA ₃ -ADH1t
pMC081	This study	[pSIVu] TCO89p-tco89 ^{K58R} -HA ₃ -ADH1t
pSF4847	This study	pSIVh-VAC8p-yEmRFP-TOR1
Software and algorithms		
ImageJ	NIH	https://imagej.nih.gov/ij/
Prism 10	GraphPad	https://www.graphpad.com/
CHARMM-36	Huang and MacKerell ¹⁰⁹	https://academiccharmm.org/
Gromacs Software version 2021	https://doi.org/10.5281/zenodo.4457591	https://www.gromacs.org/
ClueGO 2.5.3	Binda et al. ¹¹⁰	http://apps.cytoscape.org/apps/cluego
Cytoscape 3.10.3	Shannon et al. ¹¹¹	https://cytoscape.org
MaxQuant 2.0.1.0	Cox and Mann ¹¹²	https://maxquant.net/maxquant/
Omics Visualizer	Legeay et al. ¹¹³	https://cytoscape.org
Huygens Software	Huygens Remote Manager	https://www.huygens-rm.org/wp/?page_id=2
CFX Manager software	Bio-Rad	1845000

EXPERIMENTAL MODEL AND SUBJECT DETAILS

Saccharomyces cerevisiae strains used in this study are listed in the [key resources table](#). They were grown as described in [method details](#) below. Recombinant proteins were expressed in *Escherichia coli* Rosetta (DE3) and cloning procedures were carried out in *E. coli* DH5 α .

METHOD DETAILS

Yeast strains, plasmids, and growth conditions

Saccharomyces cerevisiae strains and plasmids are listed in the [key resources table](#). Gene deletions and genomically tagging were performed using the pFA6a system-based PCR-toolbox,¹¹⁴ unless otherwise stated (i.e. when clones were expressed from plasmids). Point mutations were introduced in the genome by CRISPR-Cas9, as described.^{45,107} The oligonucleotides used to generate the CRISPR-Cas9 plasmids, and the donor sequences are listed in the [key resources table](#). Strains were rendered prototrophic via transformation with centromeric plasmids listed in the [key resources table](#). Cell growth was monitored by measuring the

concentration (OD_{600nm}/mL) with a spectrophotometer. To maintain selection of plasmids, cells were pre-grown in synthetic medium devoid of leucine, histidine, uracil, adenine, and tryptophan (SD-LHUAW; 0.17% yeast nitrogen base, 0.5% ammonium sulfate, 0.2% dropout mix -LHUAW USBiological, and 2% glucose). For experiments requiring cultures in exponential phase of growth, cells were then resuspended after overnight growth in synthetic complete medium (SC; 0.17% yeast nitrogen base, 0.5% ammonium sulfate, 0.2% complete dropout mix USBiological, and 2% glucose). Starvation experiments were performed by cell filtration and transfer to a synthetic medium devoid of amino acids and ammonium sulfate (-AA; 0.17% yeast nitrogen base, and 2% glucose) and collected at the indicated time-points. For amino acid re-addition experiments, 3.3 mM glutamine was added to the cultures in -AA medium from a 50x stock in sterile water. Cells were treated with the indicated concentration of rapamycin (LC Laboratories) stored in a 1 mg/mL stock in ethanol and freshly diluted in a working solution in water to 10 μ g/mL. Treatments with MG-132 (Merck) were performed at 50 μ M final concentration (from a 1'000x concentrated stock in DMSO). As a control, the same volume of DMSO was added. Treatments with cycloheximide (AppliChem) were performed at 25 μ g/mL final concentration (from a 1'000x concentrated stock in ethanol). As a control, the same volume of ethanol was added. Strains and plasmids are available upon request.

Denaturing protein extraction and SDS-PAGE

Protein extraction from yeast cultures in denaturing conditions was performed as published.⁴⁵ Briefly, 10 mL of cell culture were mixed with trichloroacetic acid (TCA) at a final concentration of 6%. After centrifugation, the pellet was washed with cold acetone and dried in a speed-vac. The pellet was resuspended in lysis buffer (50 mM Tris-HCl [pH 7.5], 5 mM EDTA, 6 M urea, and 1% SDS), the amount being proportional to the OD_{600nm}/mL of the original cell culture. Proteins were extracted by mechanical disruption in a Precellys machine after the addition of glass beads. Subsequently, 2x sample buffer (350 mM Tris-HCl [pH 6.8], 30% glycerol, 600 mM DTT, 10% SDS, and bromophenol blue) was added to the whole-cell extract and the mix was boiled at 98°C for 5 minutes. The analysis was carried out on SDS-PAGE by loading 15 μ L of extracts on 7.5% or 9% polyacrylamide gels. The transfer on nitrocellulose membranes was performed with a Trans-Blot Turbo Transfer System (Bio-Rad) with Bjerrum Schafer-Nielsen buffer (48 mM Tris-HCl [pH 9.2], 39 mM glycine, and 20% methanol). Protein detection was carried out using custom-made phospho-specific rabbit anti-Sch9-pThr⁷³⁷ (1:10'000 in tris-buffered saline[TBS], 1% milk) and goat anti-Sch9 (1:1'000 in TBS, 5% milk) antibodies and commercial rabbit anti-Adh1 (Calbiochem, 1:50'000 in TBS, 5% milk), mouse anti-GFP (Roche, 1:3'000 in TBS, 1% milk), mouse anti-myc (Santa Cruz, 1:1'000 in TBS, 5% milk), and mouse anti-HA antibodies (ENZO, 1:1'000 in TBS, 5% milk). Band intensities from biological replicates indicated in each figure legend were quantified with ImageJ.

Drop spot assays on solid media

Cells were grown in selective liquid medium for 6 h. Cells corresponding to 1 OD_{600nm} were isolated by centrifugation and resuspended in 1 mL of sterile water. 10-fold serial dilutions were prepared in sterile water, and 5 μ L of cell suspension was spotted on the indicated solid media and left to grow for 3 days at 30°C.

Co-immunoprecipitation and SDS-PAGE

Co-immunoprecipitation was performed as published.⁴⁵ Cells were grown to exponential phase in SC, collected by filtration and frozen in liquid nitrogen. Subsequently, cells were disrupted in a Precellys homogenizer in lysis buffer (50 mM Tris-HCl [pH 7.5], 150 mM NaCl, 0.1% NP-40, 10% glycerol, Roche Phostop phosphatase inhibitor, and Roche complete protease inhibitor EDTA-free). After equilibration at the same protein concentration, immunoprecipitations were performed incubating the cleared lysates for 2 h at 4°C with prewashed GFP-Trap agarose magnetic beads (ChromoTek) or with Pierce™ anti-HA magnetic beads (Thermo Scientific). After five washes with lysis buffer, beads were resuspended in 20 μ L lysis buffer and denatured with 20 μ L of sample buffer (350 mM Tris-HCl [pH 6.8], 30% glycerol, 600 mM DTT, 10% SDS, and bromophenol blue) for 5 min at 98°C. Inputs and pull-down samples were analyzed by SDS-PAGE immunoblotting with mouse anti-GFP (Roche, 1:3'000 in TBS, 1% milk) and mouse anti-HA antibodies (ENZO, 1:1'000 in TBS, 5% milk). Band intensities from 3 biological replicates were quantified with ImageJ.

GST pulldown assays

Pulldown experiments with recombinant proteins were carried out as follows. Rosetta cells were co-transformed with plasmids expressing, or not (as indicated in Figure S4A), Gtr1, Gtr2 and GST-Tco89⁵⁸⁵⁻⁷⁹⁹ or GST-Tco89⁵⁹⁸⁵⁻⁷⁹⁹, SRTQK-AAAAA, or His₆-Kog1⁵³⁶⁻¹⁰⁸² and either GST alone or GST-Tco89⁵⁸⁵⁻⁷⁹⁹ (Figure S4B) and grown on lysogeny broth (LB) medium containing chloramphenicol, ampicillin and/or kanamycin. Overnight cultures were diluted (1:50) and grown until OD_{600} nm of 0.8. Then, 0.5 mM of isopropyl β-D-1-thiogalactopyranoside (IPTG) was added and protein expression was induced overnight at 16°C. Cells were subsequently centrifuged and resuspended in 10 mL of lysis buffer (50 mM sodium phosphate [pH 8.0], 300 mM NaCl, 0.1% NP40, and 1x Pefablock [Sigma Aldrich]), sonicated two times for 70 seconds at full speed [1'000 KJ] and centrifuged for 20 min at 4'000 g. GST pulldowns from cell extracts were carried out using 150 μ L GST magnetic beads (Genescript) for 90 min at 4°C. Aliquots of lysates (input) were taken and diluted (1:1) with sample buffer for immunoblot analyses. Beads were washed three times with lysis buffer and then two times with wash buffer (50 mM sodium phosphate [pH 8.0] and 300 mM NaCl) before being resuspended in 150 μ L of sample buffer and boiled for 5 min and analyzed by immunoblotting using anti-GST (polyclonal rabbit; Bethyl), anti-Tetra-His (monoclonal mouse; Merck), and anti-Gtr1 and anti-Gtr2 (custom made, polyclonal rabbit; Genescript) antibodies.

Split-ubiquitin yeast two-hybrid assay

The split-ubiquitin yeast two-hybrid system from Dualsystems Biotech AG was used following the manufacturer's instructions. Pib2, Gtr1, Gtr2, and Kog1 were cloned into pCabWT (bait vector) and Gtr1 (allelic full-length variants and truncated versions), Gtr2, Ego1, Ego2, Ego3, and Tco89 (allelic full-length variants and a truncated version) were cloned into pPR3N (prey vector). Combinations of these bait and prey vectors (including also empty vector controls) were transformed into WT NMY51 or isogenic egoc Δ cells as indicated. The resulting yeast strains were grown to exponential growth phase and spotted (10-fold serial dilutions) on SD-leu, trp plates (SD-LW; growth control) or SD-leu, trp, ade plates (SD-LWA; selective condition), and grown for 3 days at 30°C. Protein-protein interactions were detected as growth of the resultant strains on agar plates lacking adenine (SD-LWA). pDL2-Alg5 and pAl-Alg5 vectors were used as negative and positive controls, respectively.

In vitro phosphatase assay

Tco89-HA₃ expressing cells were grown to the exponential phase in SC, collected by filtration and frozen in liquid nitrogen. Tco89-HA₃ was immunoprecipitated using 120 µL of anti-HA magnetic beads (Pierce Thermo Fischer Scientific) from 35 mg total protein extract in lysis buffer plus inhibitors (50 mM Tris-HCl [pH 7.5], 150 mM NaCl, 0.1% NP-40, 10% glycerol, Roche Phostop phosphatase inhibitor, and Roche complete protease inhibitor EDTA-free), obtained by mechanical disruption in a Precellys homogenizer. After 5 washes with lysis buffer, the beads were split into 4 equal aliquots. Phosphatase assay on beads was carried out at 30°C for 30 min in 50 µL reactions using a commercial kit (New England Biolabs). Reactions were assembled with 10x buffer and MnCl₂, and alternatively: without enzyme, with 1 µL λ Protein Phosphatase (λPP), with λPP pre-treated for 1 h at 65°C, or inactivated by pre-treating for 1 h at 30°C with phosphatase inhibitors (Roche). After drying, the beads were resuspended in 25 µL sample buffer (350 mM Tris-HCl [pH 6.8], 30% glycerol, 600 mM DTT, 10% SDS, and bromophenol blue) and denatured for 5 min at 98°C. Anti-HA immunoprecipitates were analyzed on SDS-PAGE by immunoblotting with commercial mouse anti-HA antibodies.

Fluorescence microscopy

Yeast cells were grown in SC medium to log phase at 30°C. For amino acid starvation experiments, exponentially growing cells were filtered, washed, and resuspended in a synthetic medium devoid of ammonium sulfate and amino acids for the indicated time. Cells were imaged on an inverted spinning-disk confocal microscope (Nikon Ti-E; VisiScope CSU-W1), equipped with a dual-camera system (Hamamatsu Orca Quest (C15550-20UP) qCMOS) and a 100x, NA 1.3 oil-immersion Nikon CFI series objective. Stacks of eleven images with 0.2 µm spacing were taken. Images were then deconvolved using the remote manager (HRM) from the Huygens Software by Scientific Volume Imaging. Subcellular features were manually counted. Data in the text are presented as the average of at least 5 fields, with SD. n = total number of inspected cells.

Computational modeling

AlphaFold-multimer v2 was used to model the Kog1-Tco89-Gtr1-Gtr2 complex.¹¹⁵ To study possible interactions between the subunits, the models of Tco89 in complex with Gtr1, Gtr2, and Kog1 were initially predicted separately. A model confidence (ipmt + ptm) with a score of 0.7 was obtained for the prediction of the Tco89-Gtr1-Gtr2 complex, and a model confidence with a score of 0.8 was obtained for the prediction of the Tco89-Kog1 complex. To model the entire system, the disordered regions of Tco89 and the amino acid residues of Kog1 that are not involved in the interaction were excluded. Consequently, the amino acid residues 574-728 of Tco89, and amino acid residues 526-1082 of Kog1 were considered to predict the final model. Accordingly, 25 models of the Kog1-Tco89-Gtrs complex were produced using AlphaFold-multimer v2, setting the number of recycles to 20, and the number of iterations for the relaxed structure to 200, with a tolerance of 0.5. A final model confidence score of 0.42-0.47 was obtained. The model with the highest confidence score was selected as WT structure to run a molecular dynamics (MD) simulation. To dock the GTP and GDP molecules into Gtr1 and Gtr2, the protein database (PDB) structure of the yeast Gtr1-Gtr2 heterodimer (PDB ID: 4arz) was structurally aligned to the Kog1-Tco89-Gtr1-Gtr2 complex. The two nucleosides were placed into the pockets of Gtr1 and Gtr2 based on the structural alignment provided between the yeast model (PDB ID: 3r7w) and the mammalian one (PDB ID: 6ulg).

Molecular dynamics simulations

To simulate the Kog1-Tco89-Gtr1^{GTP}-Gtr2^{GDP} complex, it was solvated using the TIP3P water model¹¹⁶ and neutralized with a concentration of 0.15 M of sodium chloride. The steepest descent algorithm was used for the energy minimization. Subsequently, an NVT equilibration of 2 ns was performed using the v-rescale thermostat and setting the temperature at 300 K, with $\tau_T=1$ ps.¹¹⁷ An NPT (number of particles, pressure, and temperature) equilibration of 2 ns was performed using the v-rescale thermostat with a temperature of 310 K, and the Berendsen barostat, with $\tau_P=1$.¹¹⁸ A simulation of about 400 ns was produced in an NPT ensemble, with a time step of 2 fs. The v-rescale thermostat and the Parrinello-Rahman barostat were used with a $\tau_T=1$ ps, and an isotropic coupling with $\tau_P=1$ ps.¹¹⁹ The electrostatic interactions were calculated using the particle mesh Ewald method¹²⁰ with a cut-off of 1.2 nm. A cutoff of 1.2 nm was used for the van der Waals interactions. The simulation was performed using CHARMM-36 force field¹⁰⁹ and the Gromacs Software version 2021.5 (<https://doi.org/10.5281/zenodo.4457591>).

Computational analyses

The hydrogen bond analyses were performed by means of the gmx hbond tool of Gromacs Software v2021.5.5 (<https://doi.org/10.5281/zenodo.4457591>).

Chronological lifespan experiments (CLS)

Cell cultures were grown in liquid SC medium until mid-late exponential phase, then inoculated at 0.150 OD_{600nm}/mL in flasks containing medium and let grow until stationary phase (Day 0). For CLS experiments upon amino acid starvation, cells in exponential phase (0.6–0.7 OD_{600nm}/mL) were collected through centrifugation, washed with 1 volume of water and resuspended in amino acid starvation medium (Day 0). Survival of cells over time was assessed by propidium iodide staining (PI) at the indicated time points, with a Cytoflex cytofluorimeter (Beckman Coulter) and analyzed with the Cytoflex software.

RNA extraction and qRT-PCR

Cells were collected by filtration and rapidly frozen at -80°C. Then, cells were resuspended in LETS buffer (200 mM LiCl, 20 mM EDTA, 20 mM Tris-HCl [pH 7.4], and 20% SDS) and lysed on vortex with glass beads. Two steps of phenol:chloroform:isoamyl alcohol (PCI) extraction were performed. RNA was precipitated with ethanol and 0.5 M LiCl at -80°C. RNA (35 µg) was treated with 6 units of DNase I (RNase-free, Jena Bioscience) for 1 h at 37°C, followed by PCI extraction and by ethanol precipitation at -80°C. Reverse transcription of 0.5 µg of mRNAs was carried out with iScript cDNA Synthesis Kit (Bio-Rad). Quantitative real-time PCRs (qRT-PCRs) were performed in biological triplicate using the ChamQ Universal SYBR qPCR Master Mixsupermix (Vazyme) and carried out in the MiniOpticon PCR detection system (Bio-Rad). Data were normalized to those for *CDC28* and *CDC34* reference genes and organized with CFX Manager software (Bio-Rad). Primers are listed in the [key resources table](#).

TORC1 purification and kinase assay

Cells expressing Tco89-TEV-TAP were cultured in YPD medium to an optical density at 600 nm (OD₆₀₀) of 2.5. One hour before harvesting, the medium was refreshed (50 g YPD powder per liter), and TORC1 activity was further stimulated by adding 25 µg/mL cycloheximide for 10 minutes. Cells were collected by filtration, frozen in liquid nitrogen, and mechanically disrupted with the grinding machine (Mixer Mill MM 400, Retsch). The resulting powder was resuspended in lysis buffer containing 50 mM HEPES/NaOH (pH 7.5), 5 mM CHAPS, 400 mM NaCl, 1 mM EDTA, 0.5 mM DTT, 400 µM Pefabloc, and 1x Roche EDTA-free protease inhibitor cocktail. The lysate was clarified by centrifugation (16,000x g, 10 min, 4°C). TORC1 was purified by incubating the lysate with IgG-coupled Dynabeads for 2 hours at 4°C, washing the beads with wash buffer (50 mM HEPES [pH 7.5], 5 mM CHAPS, 400 mM NaCl, and 0.5 mM DTT), and cleaving TORC1 from the beads using 2% TEV protease for 1 hour at 18°C. After adding glycerol to 10% final concentration, the eluates were snap-frozen in liquid nitrogen and stored at -80°C.

For *in vitro* filter-aided kinase assays, 60 ng of purified TORC1 was added to 10-kDa molecular weight cutoff filters (Pall) and incubated for 1 hour at 30°C in kinase buffer containing 50 mM HEPES (pH 7.4), 150 mM NaCl, 0.625 mM DTT, 1x PhosSTOP (Roche), 6.25 mM MgCl₂, and 1.8 mM γ-[¹⁸O₄]-ATP (Cambridge Isotope Laboratory), with or without 6 µM of the TORC1 inhibitor wortmannin.^{46,121} The reaction was terminated by adding 8 M urea and 1 mM DTT. Protein digestion for mass spectrometry (MS) analysis was performed overnight using the filter-aided sample preparation (FASP) protocol.¹²² On the second day, peptides were eluted twice with 100 µL of 50 mM ammonium bicarbonate into fresh tubes. Eluates were acidified with trifluoroacetic acid (TFA) to a final concentration of 1% before phosphopeptide enrichment.

MS sample preparation, phosphopeptide enrichment, and LC-MS/MS analyses

Samples were processed and LC-MS/MS analyses were performed as described earlier.^{44,123} Briefly, WT (MJ5682) and isogenic tco89Δ (LD6663) strains were pre-grown in synthetic dextrose (SD) complete medium containing either non-labeled or labeled lysine and arginine variants. Exponentially growing cells were then filtered or not into SD medium without amino acids and ammonium sulfate and starved for amino acids for 30 min (see also “[yeast strains, plasmids, and growth conditions](#)”). Differentially labeled TCA-treated cell pellets were mixed, proteins extracted in 8 M urea, and digested by Lys-C (Lysyl Endopeptidase, WAKO) for 4 h at RT, followed by an overnight trypsin digestion (Promega). Resulting peptides were purified by SPE using HR-X columns in combination with C18 cartridges (Macherey-Nagel), eluates were frozen in liquid nitrogen and lyophilized overnight. Peptides were fractionated by HPLC reversed phase chromatography, fractions were acidified, frozen in liquid nitrogen, and lyophilized overnight. Peptides were suspended in 200 µL 80% acetonitrile with 1% TFA for phosphopeptide enrichment by TiO₂ beads (GL Sciences). The tip flow-through was stored at -80°C for non-phosphopeptide analysis. LC-MS/MS measurements were performed on a QExactive (QE) HF-X mass spectrometer coupled to an EasyLC 1200 nanoflow- HPLC (all Thermo Scientific). Peptides were fractionated on a fused silica HPLC-column tip (I.D. 75 mm, New Objective, self-packed with ReproSil-Pur 120 C18-AQ, 1.9 mm [Dr. Maisch] to a length of 20 cm) using a gradient of A (0.1% formic acid in water) and B (0.1% formic acid in 80% acetonitrile in water). The QE HF-X was operated in the data-dependent mode; after each MS scan (mass range m/z = 370 – 1750; resolution: 120'000 for HF-X) a maximum of twelve MS/MS scans were performed using a normalized collision energy of 25%, a target value of 5'000 and a resolution of 30'000. MS raw files were analyzed using MaxQuant (version 2.0.1.0)¹¹² using a UniProt full-length *S. cerevisiae* database (March, 2016) and common contaminants, such as keratins and enzymes used for in-gel digestion, as reference. Carbamidomethylcysteine was set as fixed modification and protein amino-terminal acetylation, serine-, threonine- and tyrosine- phosphorylation, and oxidation of

methionine were set as variable modifications. The MS/ MS tolerance was set to 20 ppm and three missed cleavages were allowed using trypsin/P as enzyme specificity. Peptide, site, and protein FDR based on a forward-reverse database were set to 0.01, minimum peptide length was set to 7, the minimum score for modified peptides was 40, and minimum number of peptides for identification of proteins was set to one, which must be unique. MS data have been deposited to the MS data have been deposited to the ProteomeXchange Consortium via the PRIDE partner repository with the dataset identifier PXD059088.^{124,125}

Phosphosites were analyzed as in⁴⁴ using a random effect model assigning each site an average effect size and its corresponding 95% confidence interval. GO-term and interaction analyses were performed with Cytoscape 3.10.3 (cytoscape.org) and ClueGO 2.5.3.,¹²⁶ STRING DB,¹²⁷ and Omics Visualizer.¹¹³ The GO cellular compartment enrichment was calculated compared to the yeast genome and GO-term fusion was used. Only pathways with a p value of 0.05% were determined as significant (Bonferroni step-down corrected).

QUANTIFICATION AND STATISTICAL ANALYSES

Statistical significance was determined from the quantification of the indicated amount of independent biological replicates (minimum 3), by using a two-tailed Student's t-test analysis. Values with a p-value lower than 0.05 were considered significantly different. The number of quantified independent replicas, the method used to express the variability and significance are indicated in the figure legends.